MATCH
Communications in Mathematical and in Computer Chemistry

MATCH Commun. Math. Comput. Chem. **78** (2017) 633-664

ISSN 0340 - 6253

Hierarchical Enumeration of Oxirane Derivatives by Using Combined–Permutation Representations

Shinsaku Fujita

Shonan Institute of Chemoinformatics and Mathematical Chemistry,
Kaneko 479-7 Ooimachi, Ashigara–Kami–Gun, Kanagawa–Ken,
258-0019 Japan

`shinsaku_fujita@nifty.com`

(Received January 17, 2017)

Abstract

Combined-permutation representations, which have been originally developed for point groups and defined as the combination of permutation representations of groups and a mirror-coset representation (S. Fujita, *MATCH Commun. Math. Comput. Chem.* **76** (2016) 379–400), are applied to group hierarchy for characterizing an oxirane skeleton. According to the group hierarchy, the point group $\boldsymbol{C}_{2v}$ (for enantiomerism), the *RS*-stereoisomeric group $\boldsymbol{C}_{2v\widetilde{\sigma}\widehat{I}}$ (for *RS*-stereoisomerism), the stereoisomeric group $\widetilde{\boldsymbol{C}}_{2v\widetilde{\sigma}\widehat{I}}$ (for stereoisomerism), and the isoskeletal group $\widetilde{\widetilde{\boldsymbol{C}}}_{2v\widetilde{\sigma}\widehat{I}}$ (for isoskeletomerism) are successively defined as combined-permutation representations by starting from respective sets of generators. Then, hierarchical enumeration of oxirane derivatives is conducted by calculating cycle indices with chirality fittingness (CI-CFs) according to Fujita's proligand method (S. Fujita, *Combinatorial Enumeration of Graphs, Three-Dimensional Structures, and Chemical Compounds*, University of Kragujevac, Faculty of Science, Kragujevac, 2013). A set of ligand-inventory functions for 3D enumerations and a single ligand-inventory function for 2D (graph) enumeration are defined to discuss interfacial behaviors between 3D structures and 2D structures (graphs). The introduction of these ligand-inventory functions into the CI-CFs provide generating functions for giving enumeration data of oxirane derivatives. These enumeration data are examined by drawing respective isomer-classification diagrams.

1 Introduction

Although several critical reviews on serious confusion in the theoretical foundations and terminology of organic chemistry have appeared [1–4], they have not fully been successful in clarifying the roots of such serious confusion. Several attempts to eliminate such serious confusion have not reached comprehensive solutions [5–7], because conceptual defects of organic chemistry have been overlooked as the roots of such serious confusion. In particular, indifference toward the concepts of *equivalence relationships* and *equivalence classes* should be mentioned as one of the conceptual defects of organic chemistry in comparison with the fact that these concepts are, in turn, fundamental in the field of mathematics [8]. As a typical example of such indifference, the classification scheme of isomers should be referred to because it suffers from serious confusion, as discussed recently [9, 10].

According to a traditional scheme of classifying isomers, isomers is subdivided into constitutional isomers (isomers different in their constitutions) and stereoisomers (isomers having the same constitution) [11], so that this subdivision results in the misleading dichotomy between constitutional isomers and stereoisomers. Further, stereoisomers is subdivided into enantiomers and diastereomers, so as to give various expressions of the misleading dichotomy between enantiomers and diastereomers, as found on page 38 of Ref. [12], page 30 of Ref. [13], and page 49 of Ref. [14]. Unfortunately, the misleading scheme of classifying isomers is widespread in the form of flowcharts, e.g., Figure 1 of Ref. [15] and Figure 21 of Ref. [16]. Such misleading flowcharts are adopted even in textbooks on organic chemistry (e.g., Figure on page 348 of Ref. [17] and Figure 5.1 of Ref. [18]), on organic stereochemistry (e.g., Figure on page 19 of Ref. [19]), as well as on inorganic stereochemistry (e.g., Figure 4.12 of Ref. [14]).

To avoid the misleading dichotomy between constitutional isomers and stereoisomers and the misleading dichotomy between enantiomers and diastereomers, a new scheme based on the concepts of equivalence relationships and equivalence classes has been proposed by the author (Fujita) [9, 10]. Thereby, a new flowchart for classifying isomers has been created in place of the traditional flowcharts described in the preceding paragraph. In particular, the new flowchart has brought about the following hierarchy of isomerism:

$$\begin{aligned}\text{enantiomerism} \subseteq RS\text{-stereoisomerism} \subseteq \text{stereoisomerism} \\ \subseteq \text{isoskeletomerism} \subseteq \text{isomerism},\end{aligned} \tag{1}$$

where the respective stages of the hierarchy connote the corresponding equivalence relationships, i.e., enantiomeric relationships, RS-stereoisomeric relationships, stereoisomeric relationships, isoskeletomeric relationships, and isomeric relationships. In comparison with the traditional scheme (i.e., enantiomerism + diastereoisomerism $\subseteq$ stereoisomerism + constitutional isomerism $\subseteq$ isomerism), the hierarchy represented by Eq. 1 contains RS-stereoisomerism [20] and isoskeletomerism [9, 10] as new matters and excludes diastereoisomerism [11] and constitutional isomerism [11] in order to assure the rationality of the new flowchart. Note that RS-stereoisomerism stems from RS-stereoisomeric relationships, which are based on RS-stereoisomeric groups algebraically or on stereoisograms as diagrammatic expressions [20]; and that isoskeletomerism stems from isoskeletomeric relationships, which are based on isoskeletal groups [9, 10].

The hierarchy of isomerism (Eq. 1) is concerned with the respective equivalence relationships, which are capable of providing the hierarchy concerning the corresponding equivalence classes:

$$\begin{aligned} &\text{a pair of enantiomers} \subseteq \text{a quadruplet of } RS\text{-stereoisomers} \subseteq \text{a set of stereoisomers} \\ &\qquad\qquad \subseteq \text{a set of isoskeletomers} \subseteq \text{a set of isomers,} \end{aligned} \tag{2}$$

where each equivalence class is permitted to be single-membered. Such a single-membered case may be emphasized by the prefix *self-*. In particular, a pair of self-enantiomers coincides to give an achiral object.

As indicated by Eq. 2, a set of isomers (or more strictly speaking, a set of isoskeletomers) consists of definite sets of stereoisomers (a single-membered set is permitted) *just enough*, so that the participation of "constitutional isomers" is rationally excluded from the hierarchy (Eq. 2). Instead, two inequivalent sets of stereoisomers are concluded to be *constitutionally anisomeric*, where the term *anisomeric* is used to emphasize the inequivalency between the two sets of stereoisomers. In addition, a set of stereoisomers consists of definite pairs of (self-)enantiomers *just enough*, so that the participation of "diastereomers" is also excluded from the hierarchy (Eq. 2). Instead, two inequivalent pairs of (self-)enantiomers are concluded to be *diastereomeric* so as to exhibit the inequivalency between the two pairs of (self-)enantiomers. The inclusion behaviors represented by Eq. 2 are diagrammatically expressed by means of isomer-classification diagrams [10].

Because the above-mentioned approaches are rather qualitative, the next task is to provide more quantitative approaches to the classification of isomers. One of the merits brought about by the addition of isoskeletomerism [9, 10] is the capability of constructing the following hierarchy of groups:

$$\begin{aligned} &\text{point groups (PG)} \subseteq RS\text{-stereoisomeric groups } (RS\text{-SIG}) \\ &\qquad\qquad \subseteq \text{stereoisomeric groups (SIG)} \subseteq \text{isoskeletal groups (ISG).} \end{aligned} \tag{3}$$

Thereby, combinatorial approach to group hierarchy for stereoskeletons of ligancy 4 has been conducted, as reported in a recent article [21]. As found by the absence of "isomeric groups" in Eq. 3, the concept of *isomerism* (Eq. 1) cannot be formulated by the action of a single group, but be interpreted by the action of one or more isoskeletal groups. Remember, for example, that the isomerism concerning the composition C^6H^6 (molecular formula C_6H_6) is formulated by considering several skeletons, e.g., a hexagonal skeleton (Kekulé's benzene) belonging to a point group $\boldsymbol{D}_{6h}$ (and the corresponding group hierarchy) and a prismane skeleton (Ladenburg's benzene) belonging to a point group $\boldsymbol{D}_{3h}$ (and the corresponding group hierarchy) [9].

The aim of this article is to examine the quantitative feasibility of the hierarchy (Eqs.1–3) by using an oxirane skeleton as a probe. Because various GAP functions [22–24] have been developed to conduct combinatorial enumeration based on Fujita's proligand method [25–28], they are applied to the oxirane skeleton for the purpose of clarifying the rationality of the hierarchy represented by Eqs.1–3.

2 Group hierarchy for an oxirane skeleton

2.1 Point group $\boldsymbol{C}_{2v}$ for enantiomerism

Suppose that the four positions of an oxirane skeleton **1** are numbered sequentially, as shown by the projection formula in Figure 1 (left). The oxirane skeleton **1** belongs to the point group $\boldsymbol{C}_{2v}$, the elements (operations) of which are illustrated in its top view **2** depicted in Figure 1 (right).

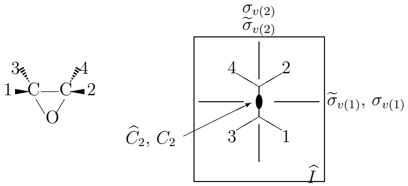

1 **2**

Figure 1. Oxirane skeleton (left) and its top view (right) with the elements of the point group $\boldsymbol{C}_{2v}$ and the *RS*-stereoisomeric group $\boldsymbol{C}_{2v\widetilde{\sigma}\widehat{I}}$

Suppose that the four positions of **1** is regarded as the following set:

$$\mathbf{X} = \{1, 2, 3, 4\}. \tag{4}$$

Then, the action of $\boldsymbol{C}_{2v}$ on the set $\mathbf{X}$ is represented by a right-coset representation

$(\boldsymbol{C}_1\backslash)\boldsymbol{C}_{2v}$, which is expressed in terms of products of cycles:

$$\begin{aligned} \boldsymbol{C}_{2v} &= \{I, C_2, \sigma_{v(1)}, \sigma v(2)\} \\ &\sim \{(1)(2)(3)(4), (1\ 4)(2\ 3), \overline{(1\ 2)(3\ 4)}, \overline{(1\ 3)(2\ 4)}\} = (\boldsymbol{C}_1\backslash)\boldsymbol{C}_{2v}, \end{aligned} \tag{5}$$

where an overline represents a ligand reflection. Note that the right-coset representation $(\boldsymbol{C}_1\backslash)\boldsymbol{C}_{2v}$ is adopted here in place of the corresponding left-coset representation $\boldsymbol{C}_{2v}(/\boldsymbol{C}_1)$, because the GAP system adopts right-coset representations as standards and presumes that the multiplication of permutations is executed from left to right.

To treat such right-coset representations systematically by computer, the expressions with an overline should be transformed to computer-oriented representations. As such computer-oriented representations, the author (Fujita) has proposed the combined-permutation representation $\boldsymbol{P}^{(\mathbf{X}_\chi)}_{\boldsymbol{C}_{2v}}$ (`C2v`) by combining the coset representation $(\boldsymbol{C}_1\backslash)\boldsymbol{C}_{2v}$ (or $\boldsymbol{C}_{2v}(/\boldsymbol{C}_1)$) with a mirror-permutation representation, which acts on the domain $\chi = \{5, 6\}$ to indicate a mirror permutation corresponding to an overline [22]. Thereby, the respective elements of Eq. 5 are represented as follows:

$$\begin{array}{ccc} (\boldsymbol{C}_1\backslash)\boldsymbol{C}_{2v} & \boldsymbol{P}^{(\mathbf{X}_\chi)}_{\boldsymbol{C}_{2v}} & \texttt{C2v} \\ \hline (1)(2)(3)(4) & (1)(2)(3)(4)(5)(6) & () \\ (1\ 4)(2\ 3) & (1\ 4)(2\ 3)(5)(6) & (1,4)(2,3) \\ \overline{(1\ 2)(3\ 4)} & (1\ 2)(3\ 4)(5\ 6) & (1,2)(3,4)(5,6) \\ \overline{(1\ 3)(2\ 4)} & (1\ 3)(2\ 4)(5\ 6) & (1,3)(2,4)(5,6) \end{array} \tag{6}$$

where the last `C2v`-column collects concrete expressions with omitting 1-cycles and adding commas, which are used during the execution of the GAP system. The crux of the present approach is that the combined-permutation representation $\boldsymbol{P}^{(\mathbf{X}_\chi)}_{\boldsymbol{C}_{2v}}$ (`C2v`) is regarded as a permutation group of degree 6 (= 4 + 2). Thereby, the group-theoretical properties of the point group $\boldsymbol{C}_{2v}$ are systematically revealed by computer (through the GAP system).

The point group $\boldsymbol{C}_{2v}$ is decomposed by its subgroup $\boldsymbol{C}_2$ as follows:

$$\boldsymbol{C}_{2v} = \boldsymbol{C}_2 + \boldsymbol{C}_2\sigma_{v(1)}. \tag{7}$$

Let the symbol `elm_C2` be a GAP list for the set of the elements of $\boldsymbol{C}_2$. Then, the multiplication of $\sigma_{v(1)}$ from the right is calculated to be `elm_C2`$*(1,2)(3,4)(5,6)$, which provides a GAP list corresponding to the right-coset $\boldsymbol{C}_2\sigma_{v(1)}$ (Eq. 7). The concatenated list `elm_C2v` (cf. Eq. 6) is constructed by using the GAP function `Concatenation`, as found in the following code:

```
gap> elm_C2 := [(), (1,4)(2,3)];
[ (), (1,4)(2,3) ]
gap> elm_C2v := Concatenation(elm_C2, elm_C2*(1,2)(3,4)(5,6));
[ (), (1,4)(2,3), (1,2)(3,4)(5,6), (1,3)(2,4)(5,6) ]
gap> C2v := AsGroup(elm_C2v);
Group([ (1,2)(3,4)(5,6), (1,3)(2,4)(5,6) ])
```

The concatenated list `elm_C2v` works as a group by using the GAP function `AsGroup`, so that it is transformed into a group constructed by the GAP function `Group` with a set of generators, i.e., $[(1,2)(3,4)(5,6),(1,3)(2,4)(5,6)]$.

The $\boldsymbol{C}_{2v}$-part of Table 1 shows another construction of the combined-permutation representation $\boldsymbol{P}^{(\mathbf{X}_\chi)}_{\boldsymbol{C}_{2v}}$ (`C2v`), where the list `elm_C2v` (cf. Eq. 6) is directly input after the command prompt `gap>`.

Table 1. Group Hierarchy for Characterizing an Oxirane Skeleton

group — list of elements for constructing a group

$\boldsymbol{C}_{2v}$
(point group)
order: 4

```
gap> #Point group;;
gap> elm_C2v := [(), (1,4)(2,3), (1,2)(3,4)(5,6), (1,3)(2,4)(5,6)];
[ (), (1,4)(2,3), (1,2)(3,4)(5,6), (1,3)(2,4)(5,6) ]
gap> C2v := AsGroup(elm_C2v);
Group([ (1,2)(3,4)(5,6), (1,3)(2,4)(5,6) ])
gap> IsEqualSet(elm_C2v, Elements(C2v));
true
```

$\boldsymbol{C}_{2v\widetilde{\sigma}\widehat{I}}$
(RS-stereo-isomeric group)
order: 8

```
gap> #RS-stereoisomeric group;;
gap> elm_C2vsI := Concatenation(elm_C2v, elm_C2v*(1,2)(3,4));
[ (), (1,4)(2,3), (1,2)(3,4)(5,6), (1,3)(2,4)(5,6),
(1,2)(3,4), (1,3)(2,4), (5,6), (1,4)(2,3)(5,6) ]
gap> C2vsI := AsGroup(elm_C2vsI);
Group([ (5,6), (1,2)(3,4), (1,3)(2,4) ])
gap> IsEqualSet(elm_C2vsI, Elements(C2vsI));
true
```

$\widetilde{\boldsymbol{C}}_{2v\widetilde{\sigma}\widehat{I}}$
(stereoisomeric group)
order: 16

```
gap> #Stereoisomeric group;;
gap> elm_cC2vsI := Concatenation(elm_C2vsI, elm_C2vsI*(2,4));
[ (), (1,4)(2,3), (1,2)(3,4)(5,6), (1,3)(2,4)(5,6),
(1,2)(3,4), (1,3)(2,4), (5,6), (1,4)(2,3)(5,6),
(2,4), (1,2,3,4), (1,4,3,2)(5,6), (1,3)(5,6),
(1,4,3,2), (1,3), (2,4)(5,6), (1,2,3,4)(5,6) ]
gap> cC2vsI := AsGroup(elm_cC2vsI);
Group([ (5,6), (2,4), (1,2)(3,4) ])
gap> IsEqualSet(elm_cC2vsI, Elements(cC2vsI));
true
```

$\widetilde{\widetilde{\boldsymbol{C}}}_{2v\widetilde{\sigma}\widehat{I}}$
(isoskeletal group)
order: 48

```
gap> #Isoskeletal group;;
gap> elm_ccC2vsI := Concatenation(elm_cC2vsI, elm_cC2vsI*(2,3),
     ↪ elm_cC2vsI*(3,4));
[ (), (1,4)(2,3), (1,2)(3,4)(5,6), (1,3)(2,4)(5,6),
(1,2)(3,4), (1,3)(2,4), (5,6), (1,4)(2,3)(5,6),
(2,4), (1,2,3,4), (1,4,3,2)(5,6), (1,3)(5,6),
(1,4,3,2), (1,3), (2,4)(5,6), (1,2,3,4)(5,6),

(2,3), (1,4), (1,3,4,2)(5,6), (1,2,4,3)(5,6),
(1,3,4,2), (1,2,4,3), (2,3)(5,6), (1,4)(5,6),
(2,4,3), (1,3,4), (1,4,2)(5,6), (1,2,3)(5,6),
(1,4,2), (1,2,3), (2,4,3)(5,6), (1,3,4)(5,6),

(3,4), (1,3,2,4), (1,2)(5,6), (1,4,2,3)(5,6),
(1,2), (1,4,2,3), (3,4)(5,6), (1,3,2,4)(5,6),
(2,3,4), (1,2,4), (1,3,2)(5,6), (1,4,3)(5,6),
(1,3,2), (1,4,3), (2,3,4)(5,6), (1,2,4)(5,6) ]
gap> ccC2vsI := AsGroup(elm_ccC2vsI);
Group([ (5,6), (3,4), (2,3), (1,2) ])
gap> IsEqualSet(elm_ccC2vsI, Elements(ccC2vsI));
true
```

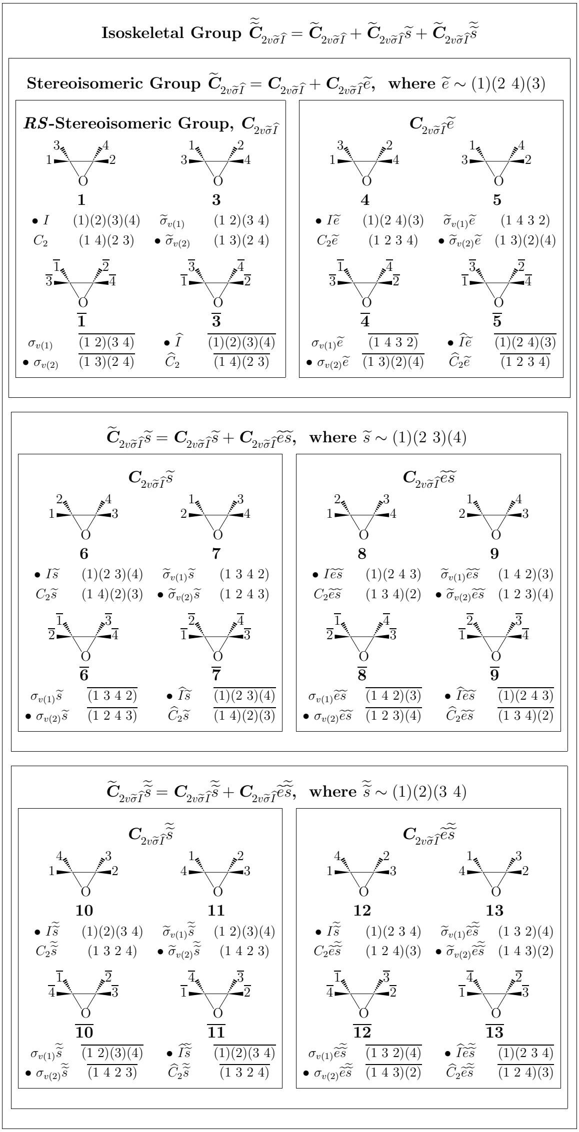

Figure 2. *RS*-Stereoisomeric groups, stereoisomeric groups, and isoskeletal groups for an oxirane skeleton. Each operation with a bullet symbol is selected as a representative to draw the corresponding skeleton. This figure is cited from [29] after the modification of left cosets into right cosets in accord with the standards of the GAP system.

The elements of the combined-permutation representation $\boldsymbol{P}^{(\mathbf{X}\chi)}_{\boldsymbol{C}_{2v}}$ (`C2v`) appearing in the $\boldsymbol{C}_{2v}$-part of Table 1 correspond to a pair of enantiomeric skeletons (**1** and $\overline{\mathbf{1}}$) shown in Figure 2. Each skeleton of the enantiomeric pair is drawn in accord with an element with a bullet symbol, which is selected as a representative of the corresponding coset appearing in Eq. 7.

It should be noted that the mirror-numbered skeleton $\overline{\mathbf{1}}$ contains locant numbers with an overline. For the purpose of clarifying the correspondence between the elements $\boldsymbol{P}^{(\mathbf{X}\chi)}_{\boldsymbol{C}_{2v}}$ (`C2v`) and the locant numbers, each element of $\boldsymbol{P}^{(\mathbf{X}\chi)}_{\boldsymbol{C}_{2v}}$ (`C2v`) is converted into the corresponding permutation of the coset representation $(\boldsymbol{C}_1\backslash)\boldsymbol{C}_{2v}$ in Figure 2 (cf. Eq. 6).

2.2 *RS*–stereoisomeric group $\boldsymbol{C}_{2v\widetilde{\sigma}\widehat{I}}$ for *RS*–stereoisomerism

The RS-stereoisomeric group $\boldsymbol{C}_{2v\widetilde{\sigma}\widehat{I}}$ is constructed by starting from the point group $\boldsymbol{C}_{2v}$ according to the following coset decomposition:

$$\boldsymbol{C}_{2v\widetilde{\sigma}\widehat{I}} = \boldsymbol{C}_{2v} + \boldsymbol{C}_{2v}\widetilde{\sigma}_{v(1)}. \tag{8}$$

As shown in the $\boldsymbol{C}_{2v\widetilde{\sigma}\widehat{I}}$-part of Table 1, the list of elements contained in the right coset $\boldsymbol{C}_{2v}\widetilde{\sigma}_{v(1)}$ of Eq. 8 is calculated by placing `elm_C2v * (1,2)(3,4)`. Then, the list of elements `elm_C2vsI` is calculated by using the GAP function `Concatenation`, so as to give the combined-permutation representation $\boldsymbol{P}^{(\mathbf{X}\chi)}_{\boldsymbol{C}_{2v\widetilde{\sigma}\widehat{I}}}$ (`C2vsI`).

The resulting RS-stereoisomeric group $\boldsymbol{C}_{2v\widetilde{\sigma}\widehat{I}}$ controls a stereoisogram containing the quadruplet of skeletons (**1**, $\overline{\mathbf{1}}$, **3**, and $\overline{\mathbf{3}}$), as shown in the $\boldsymbol{C}_{2v\widetilde{\sigma}\widehat{I}}$-block of Figure 2. The pair of enantiomers $\mathbf{1}/\overline{\mathbf{1}}$ corresponds to the coset $\boldsymbol{C}_{2v}$ $(= \boldsymbol{C}_{2v}I)$, while the pair of enantiomers $\mathbf{3}/\overline{\mathbf{3}}$) corresponds to the coset $\boldsymbol{C}_{2v}\widetilde{\sigma}_{v(1)}$ appearing in Eq. 8.

According to general properties of RS-stereoisomeric groups and stereoisograms [20,30, 31], the RS-stereoisomeric group $\boldsymbol{C}_{2v\widetilde{\sigma}\widehat{I}}$ has a subgroup of half size, i.e., an RS-permutation group $\boldsymbol{C}_{2\widetilde{\sigma}}$ $(= \{I, C_2, \widetilde{\sigma}_{v(1)}, \widetilde{\sigma}_{v(2)}\})$, so that an alternative coset decomposition is obtained:

$$\boldsymbol{C}_{2v\widetilde{\sigma}\widehat{I}} = \boldsymbol{C}_{2\widetilde{\sigma}} + \boldsymbol{C}_{2\widetilde{\sigma}}\sigma_{v(1)}. \tag{9}$$

The two cosets of Eq. 9 correspond respectively to a pair of RS-diastereomeric skeletons $\mathbf{1}/\mathbf{3}$ and another pair of RS-diastereomeric skeletons $\overline{\mathbf{1}}/\overline{\mathbf{3}}$.

The RS-stereoisomeric group $\boldsymbol{C}_{2v\widetilde{\sigma}\widehat{I}}$ is further considered to have a ligand-reflection group $\boldsymbol{C}_{2\widehat{I}}$ $(= \{I, C_2, \widehat{I}, \widehat{C}_2\})$ as a subgroup of half size. As a result, a further coset decomposition is obtained:

$$\boldsymbol{C}_{2v\widetilde{\sigma}\widehat{I}} = \boldsymbol{C}_{2\widehat{I}} + \boldsymbol{C}_{2\widehat{I}}\sigma_{v(1)}. \tag{10}$$

The two cosets of Eq. 10 correspond respectively to a pair of holantimeric skeletons $\mathbf{1}/\overline{\mathbf{3}}$ and another pair of holantimeric skeletons $\mathbf{3}/\overline{\mathbf{1}}$.

2.3 Stereoisomeric group $\widetilde{\boldsymbol{C}}_{2v\widetilde{\sigma}\widehat{I}}$ for stereoisomerism

The stereoisomeric group $\widetilde{\boldsymbol{C}}_{2v\widetilde{\sigma}\widehat{I}}$ is constructed in a nested fashion by starting from the *RS*-stereoisomeric group $\boldsymbol{C}_{2v\widetilde{\sigma}\widehat{I}}$ according to the following coset decomposition:

$$\widetilde{\boldsymbol{C}}_{2v\widetilde{\sigma}\widehat{I}} = \boldsymbol{C}_{2v\widetilde{\sigma}\widehat{I}} + \boldsymbol{C}_{2v\widetilde{\sigma}\widehat{I}}\widetilde{e}, \tag{11}$$

where the symbol $\widetilde{e}$ represents a pseudo-rotation which causes *cis/trans*-isomerization.

As shown in the $\widetilde{\boldsymbol{C}}_{2v\widetilde{\sigma}\widehat{I}}$-part of Table 1, the list of elements contained in the right coset $\boldsymbol{C}_{2v\widetilde{\sigma}\widehat{I}}\widetilde{e}$ of Eq. 11 is calculated by placing `elm_C2vsI * (2,4)`. Then, the list of elements `elm_cC2vsI` is calculated by using the GAP function `Concatenation`, so as to give the combined-permutation representation $\boldsymbol{P}^{(\mathbf{x}_X)}_{\widetilde{\boldsymbol{C}}_{2v\widetilde{\sigma}\widehat{I}}}$ (`cC2vsI`).

The resulting stereoisomeric group $\widetilde{\boldsymbol{C}}_{2v\widetilde{\sigma}\widehat{I}}$ controls a set of two stereoisograms (the $\boldsymbol{C}_{2v\widetilde{\sigma}\widehat{I}}$-block and the $\boldsymbol{C}_{2v\widetilde{\sigma}\widehat{I}}\widetilde{e}$-block), which is contained in the $\widetilde{\boldsymbol{C}}_{2v\widetilde{\sigma}\widehat{I}}$-block of Figure 2. The first stereoisogram with a quadruplet of *RS*-stereoisomers, i.e., $\mathbf{1}/\overline{\mathbf{1}}/\mathbf{3}/\overline{\mathbf{3}}$ in the $\boldsymbol{C}_{2v\widetilde{\sigma}\widehat{I}}$-block, corresponds to the first cost $\boldsymbol{C}_{2v\widetilde{\sigma}\widehat{I}}$ ($= \boldsymbol{C}_{2v\widetilde{\sigma}\widehat{I}}I$), which appears in the right-hand side of Eq. 11. On the other hand, the second stereoisogram with a quadruplet of *RS*-stereoisomers, i.e., $\mathbf{4}/\overline{\mathbf{4}}/\mathbf{5}/\overline{\mathbf{5}}$ in the $\boldsymbol{C}_{2v\widetilde{\sigma}\widehat{I}}\widetilde{e}$-block, corresponds to the second coset $\boldsymbol{C}_{2v\widetilde{\sigma}\widehat{I}}\widetilde{e}$, which appears in the right-hand side of Eq. 11.

The stabilizer of the first coset $\boldsymbol{C}_{2v\widetilde{\sigma}\widehat{I}}I$ is the subgroup $\boldsymbol{C}_{2v\widetilde{\sigma}\widehat{I}}$ itself. On the other hand, the stabilizer of the second coset $\boldsymbol{C}_{2v\widetilde{\sigma}\widehat{I}}\widetilde{e}$ of Eq.11 is calculated as follows:

```
gap> stab_C2vsI_e := AsGroup((2,4)*elm_C2vsI*(2,4));
Group([ (5,6), (1,2)(3,4), (1,3)(2,4) ])
gap> IsomorphismGroups(C2vsI,stab_C2vsI_e);
[ (5,6), (1,2)(3,4), (1,3)(2,4) ] -> [ (5,6), (1,2)(3,4), (1,3)(2,4) ]
```

This means that the stabilizer `stab_C2vsI_e` of the second coset $\boldsymbol{C}_{2v\widetilde{\sigma}\widehat{I}}\widetilde{e}$ is equal to the subgroup $\boldsymbol{C}_{2v\widetilde{\sigma}\widehat{I}}$ (`C2vsI`).

2.4 Isoskeletal group $\widetilde{\widetilde{\boldsymbol{C}}}_{2v\widetilde{\sigma}\widehat{I}}$ for isoskeletomerism

The isoskeletal group $\widetilde{\widetilde{\boldsymbol{C}}}_{2v\widetilde{\sigma}\widehat{I}}$ is constructed in a nested fashion by starting from the stereoisomeric group $\widetilde{\boldsymbol{C}}_{2v\widetilde{\sigma}\widehat{I}}$ according to the following coset decomposition:

$$\widetilde{\widetilde{\boldsymbol{C}}}_{2v\widetilde{\sigma}\widehat{I}} = \widetilde{\boldsymbol{C}}_{2v\widetilde{\sigma}\widehat{I}} + \widetilde{\boldsymbol{C}}_{2v\widetilde{\sigma}\widehat{I}}\widetilde{s} + \widetilde{\boldsymbol{C}}_{2v\widetilde{\sigma}\widehat{I}}\widetilde{\widetilde{s}}, \tag{12}$$

where the symbols $\widetilde{s}$ ($\sim$ (2 3)) and $\widetilde{\widetilde{s}}$ ($\sim$ (3 4)) represent skeletal detaching-attaching operations which derive isoskeletomeric skeletons.

As shown in the $\widetilde{\widetilde{\boldsymbol{C}}}_{2v\widetilde{\sigma}\widehat{I}}$-part of Table 1, the list of elements contained in the right coset $\widetilde{\boldsymbol{C}}_{2v\widetilde{\sigma}\widehat{I}}\widetilde{s}$ of Eq. 12 is calculated by placing `elm_cC2vsI * (2,3)`; and the list of elements contained in the right coset $\widetilde{\boldsymbol{C}}_{2v\widetilde{\sigma}\widehat{I}}\widetilde{\widetilde{s}}$ of Eq. 12 is calculated by placing `elm_cC2vsI *`

`(3,4)`. Then, the list of elements `elm_ccC2vsI` is calculated by using the GAP function `Concatenation`, so as to give the combined-permutation representation $\boldsymbol{P}^{(\mathbf{X}_\chi)}_{\widetilde{\widetilde{\boldsymbol{C}}}_{2v\widetilde{\sigma}\widehat{I}}}$ (`ccC2vsI`).

The set of 24 oxirane skeletons of Figure 2 are equivalent under the action of the isoskeletal group $\widetilde{\widetilde{\boldsymbol{C}}}_{2v\widetilde{\sigma}\widehat{I}}$ (Eq. 12), so that the set is an equivalence class to be counted once under $\widetilde{\widetilde{\boldsymbol{C}}}_{2v\widetilde{\sigma}\widehat{I}}$. These 24 oxirane skeletons of Figure 2 are divided into three blocks in accord with the coset decomposition represented by Eq. 12, i.e., the $\widetilde{\boldsymbol{C}}_{2v\widetilde{\sigma}\widehat{I}}$-block at the top of Figure 2, the $\widetilde{\boldsymbol{C}}_{2v\widetilde{\sigma}\widehat{I}}\widetilde{e}$-block at the middle, and the $\widetilde{\boldsymbol{C}}_{2v\widetilde{\sigma}\widehat{I}}\widetilde{\widetilde{s}}$-block at the bottom. This division means that the one set of isoskeletomeric skeletons consists of three sets of stereoisomeric skeletons corresponding to these three blocks.

The first coset $\widetilde{\boldsymbol{C}}_{2v\widetilde{\sigma}\widehat{I}}$ $(= \widetilde{\boldsymbol{C}}_{2v\widetilde{\sigma}\widehat{I}}I)$ of Eq. 12 corresponds to a set of stereoisomeric skeletons, which consists of two sets of stereoisograms shown in the $\widetilde{\boldsymbol{C}}_{2v\widetilde{\sigma}\widehat{I}}$-block of Figure 2. The second coset $\widetilde{\boldsymbol{C}}_{2v\widetilde{\sigma}\widehat{I}}\widetilde{s}$ of Eq. 12 corresponds to another set of stereoisomeric skeletons, which consists of two sets of stereoisograms shown in the $\widetilde{\boldsymbol{C}}_{2v\widetilde{\sigma}\widehat{I}}\widetilde{e}$-block of Figure 2. The third coset $\widetilde{\boldsymbol{C}}_{2v\widetilde{\sigma}\widehat{I}}\widetilde{\widetilde{s}}$ of Eq. 12 corresponds to one more set of stereoisomeric skeletons, which consists of two sets of stereoisograms shown in the $\widetilde{\boldsymbol{C}}_{2v\widetilde{\sigma}\widehat{I}}\widetilde{\widetilde{s}}$-block of Figure 2.

The stabilizer of the first coset $\widetilde{\boldsymbol{C}}_{2v\widetilde{\sigma}\widehat{I}}$ $(= \widetilde{\boldsymbol{C}}_{2v\widetilde{\sigma}\widehat{I}}I)$ of Eq. 12 is the subgroup $\widetilde{\boldsymbol{C}}_{2v\widetilde{\sigma}\widehat{I}}$ (`cC2vsI`) itself. On the other hand, the stabilizer (`stab_cC2vsI_s`) of the second coset $\widetilde{\boldsymbol{C}}_{2v\widetilde{\sigma}\widehat{I}}\widetilde{s}$ and the stabilizer (`stab_cC2vsI_ss`) of the third coset $\widetilde{\boldsymbol{C}}_{2v\widetilde{\sigma}\widehat{I}}\widetilde{\widetilde{s}}$ are calculated as follows:

```
gap> stab_cC2vsI_s := AsGroup((2,3)*elm_cC2vsI*(2,3));
Group([ (5,6), (3,4), (1,2), (1,3)(2,4) ])
gap> IsomorphismGroups(cC2vsI,stab_cC2vsI_s);
[ (5,6), (2,4), (1,2)(3,4) ] -> [ (5,6), (3,4), (1,3)(2,4) ]
gap> stab_cC2vsI_ss := AsGroup((3,4)*elm_cC2vsI*(3,4));
Group([ (5,6), (2,3), (1,2)(3,4) ])
gap> IsomorphismGroups(cC2vsI,stab_cC2vsI_ss);
[ (5,6), (2,4), (1,2)(3,4) ] -> [ (5,6), (2,3), (1,2)(3,4) ]
```

The GAP function `IsomorphismGroups` indicates that the latter stabilizers are isomorphic to the subgroup $\widetilde{\boldsymbol{C}}_{2v\widetilde{\sigma}\widehat{I}}$ (`cC2vsI`). These three stabilizers (`cC2vsI`, `stab_cC2vsI_s`, and `stab_cC2vsI_ss`) are conjugate under the isoskeletal group $\widetilde{\widetilde{\boldsymbol{C}}}_{2v\widetilde{\sigma}\widehat{I}}$ (`ccC2vsI`) shown in Eq. 12, as confirmed by the following output:

```
gap> ConjugateSubgroups(ccC2vsI, cC2vsI);
[ Group([ (5,6), (2,4), (1,2)(3,4) ]), Group([ (5,6), (2,3), (1,2)(3,4) ]),
  Group([ (5,6), (3,4), (1,3)(2,4) ]) ]
```

The isoskeletal group $\widetilde{\widetilde{\boldsymbol{C}}}_{2v\widetilde{\sigma}\widehat{I}}$ (Eq. 12) is isomorphic to the reflective symmetric group $\boldsymbol{S}^{[4]}_{\sigma\widehat{I}}$ (order: 48), which is derived from the symmetric group of degree 4 ($\boldsymbol{S}^{[4]}$). This isomorphism is confirmed as follows:

```
gap> ccC2vsI := Group([ (5,6), (3,4), (2,3), (1,2) ]);
Group([ (5,6), (3,4), (2,3), (1,2) ])
gap> S4sI := Group([(1,2,3,4), (1,2), (5,6)]);
Group([ (1,2,3,4), (1,2), (5,6) ])
gap> IsEqualSet(Elements(ccC2vsI), Elements(S4sI));
true
```

Note that, because the set of generators for $\boldsymbol{S}^{[4]}$ is determined to be $[(1,2,3,4),(1,2)]$, the addition of a mirror-permutation `(5,6)` to the generator set gives $\boldsymbol{S}^{[4]}_{\sigma\widehat{I}}$ (`S4sI`).

3 Hierarchical enumeration of oxirane derivatives

Hierarchical enumeration of oxirane derivatives is conducted by extending Fujita's proligand method [25–28], which has been originally developed for point groups. The procedures of calculating cycle indices with chirality fittingness (CI-CFs) for point groups are also effective to the hierarchical enumeration.

3.1 Calculation of CI-CFs

A manual calculation of a cycle index with chirality fittingness (CI-CF) is based on the examination of the cycle structures of respective elements. For example, the point group $\boldsymbol{C}_2$ ($\sim \{(1)(2)(3)(4), (1\ 4)(2\ 3)\}$, cf. Eq. 6) has two permutations with cycle structures 1^4 and 2^2, where 1-cycles and 2-cycles are determined to be hemispheric according to Fujita's proligand method [25–28]. These cycles are characterized by sphericity indices (SIs), i.e., b_d ($d = 1, 2$). Thereby, the corresponding products of sphericity indices (PSIs) are determined to be $\{b_1^4, b_2^2\}$. These PSIs are summed up and divided by the order of the point group $\boldsymbol{C}_2$ (order: $|\boldsymbol{C}_2| = 2$), so as to give the following CI-CF:

$$\text{CI-CF}(\boldsymbol{C}_2, b_d) = \frac{1}{2}(b_1^4 + b_2^2). \tag{13}$$

By developing the combined-permutation representation [22], the manual calculation described in the preceding paragraph has been systematized to develop the GAP function `CalcConjClassCICF` for calculating CI-CFs [23]. The CI-CF($\boldsymbol{C}_2, b_d$) (`CICF_C2`) is calculated by executing the following commands:

```
gap> Read("c:/fujita0/fujita2016/C2vsI-GAP/calc-GAP/CICFgenCC.gapfunc");
gap> C2 := Group([(1,4)(2,3)]);
Group([ (1,4)(2,3) ])
gap> Print("C2␣:=␣", C2, "\n");
C2 := Group( [ (1,4)(2,3) ] )
gap> Print("Order␣:=␣", Size(C2), "\n");
Order := 2
gap> Print("CICF_C2␣:=␣", CalcConjClassCICF(C2, 4, 6), "\n");
CICF_C2 := 1/2*b_1^4+1/2*b_2^2
```

Note that the GAP function `CalcConjClassCICF` is stored in the file `CICFgenCC.gapfunc`, the source list of which has been published as an appendix [23]. Another GAP function `CalcCICF` for calculating CI-CFs has been also reported as an appendix [22].

Table 2. CI-CFs for Characterizing an Oxirane Skeleton

group — `Group` due to a list of generators, order, CI-CF

$\boldsymbol{C}_2$ (point group)

```
C2 := Group( [ (1,4)(2,3) ] )
Order := 2
CICF_C2 := 1/2*b_1^4+1/2*b_2^2
```

$\boldsymbol{C}_{2v}$ (point group)

```
C2v := Group( [ (1,2)(3,4)(5,6), (1,3)(2,4)(5,6) ] )
Order := 4
CICF_C2v := 1/4*b_1^4+1/4*b_2^2+1/2*c_2^2
```

$\boldsymbol{C}_{2v\widetilde{\sigma}\widehat{I}}$ (RS-stereoisomeric group)

```
C2vsI := Group( [ (5,6), (1,2)(3,4), (1,3)(2,4) ] )
Order := 8
CICF_C2vsI := 1/8*b_1^4+1/8*a_1^4+3/8*b_2^2+3/8*c_2^2
```

$\widetilde{\boldsymbol{C}}_{2v\widetilde{\sigma}\widehat{I}}$ (stereoisomeric group)

```
cC2vsI := Group( [ (5,6), (2,4), (1,2)(3,4) ] )
Order := 16
CICF_cC2vsI := 1/16*b_1^4+1/16*a_1^4+1/8*b_1^2*b_2
               +1/8*c_2*a_1^2+3/16*b_2^2+3/16*c_2^2+1/8*b_4+1/8*c_4
```

$\widetilde{\widetilde{\boldsymbol{C}}}_{2v\widetilde{\sigma}\widehat{I}}$ (isoskeletal group)

```
ccC2vsI := Group( [ (5,6), (3,4), (2,3), (1,2) ] )
Order := 48
CICF_ccC2vsI := 1/48*b_1^4+1/48*a_1^4+1/8*b_1^2*b_2
                +1/8*c_2*a_1^2+1/6*b_1*b_3+1/16*b_2^2+1/16*c_2^2
                +1/6*a_1*a_3+1/8*b_4+1/8*c_4
```

The CI-CFs for the groups of the group hierarchy listed in Table 1 are calculated in a similar way by using the GAP function `CalcConjClassCICF`. Note that the generation of each group depends on the GAP function `Group` with a set of generators, which has been obtained by the GAP function `AsGroup` and listed in Table 1. The resulting CI-CFs are collected in Table 2, i.e., CI-CF($\boldsymbol{C}_{2v}, \$_d$) (`CICF_C2v`), CI-CF($\boldsymbol{C}_{2v\widetilde{\sigma}\widehat{I}}, \$_d$) (`CICF_C2vsI`), CI-CF($\widetilde{\boldsymbol{C}}_{2v\widetilde{\sigma}\widehat{I}}, \$_d$) (`cCICF_C2vsI`), and CI-CF($\widetilde{\widetilde{\boldsymbol{C}}}_{2v\widetilde{\sigma}\widehat{I}}, \$_d$) (`ccCICF_C2vsI`), where the symbol $\$_d$ represents a_d, c_d, or b_d.

3.2 Enumerations under the point groups $\boldsymbol{C}_2$ and $\boldsymbol{C}_{2v}$ as well as under the $\boldsymbol{RS}$–stereoisomeric group $\boldsymbol{C}_{2v\widetilde{\sigma}\widehat{I}}$

3.2.1 Ligand–inventory functions for point groups and $\boldsymbol{RS}$–stereoisomeric groups

For the purpose of enumerating oxirane derivatives, we consider the following ligand inventory for 3D enumeration:

$$\boldsymbol{L} = \{\mathrm{A}, \mathrm{B}, \mathrm{C}, \mathrm{D}; \mathrm{p}, \overline{\mathrm{p}}, \mathrm{q}, \overline{\mathrm{q}}, \mathrm{r}, \overline{\mathrm{r}}, \mathrm{s}, \overline{\mathrm{s}}\}, \tag{14}$$

where the uppercase letters A, B, C, and D represent achiral proligands, while a pair of lowercase letters p/$\overline{\mathrm{p}}$, q/$\overline{\mathrm{q}}$, r/$\overline{\mathrm{r}}$, or s/$\overline{\mathrm{s}}$ represents an enantiomeric pair of chiral proligands in isolation (when detached).

Suppose that an oxirane skeleton **1** (Figure 1) belongs to the point group $\boldsymbol{C}_2$ (or $\boldsymbol{C}_{2v}$) and that its four positions accommodate a set of four proligands selected from the ligand inventory $\boldsymbol{L}$ (Eq. 14). According to Fujita's proligand method [25–28], the following set of ligand-inventory functions are adopted:

$$a_d = \mathrm{A}^d + \mathrm{B}^d + \mathrm{C}^d + \mathrm{D}^d \tag{15}$$

$$c_d = \mathrm{A}^d + \mathrm{B}^d + \mathrm{C}^d + \mathrm{D}^d + 2\mathrm{p}^{d/2}\overline{\mathrm{p}}^{d/2} + 2\mathrm{q}^{d/2}\overline{\mathrm{q}}^{d/2} + 2\mathrm{r}^{d/2}\overline{\mathrm{r}}^{d/2} + 2\mathrm{s}^{d/2}\overline{\mathrm{s}}^{d/2} \tag{16}$$

$$b_d = \mathrm{A}^d + \mathrm{B}^d + \mathrm{C}^d + \mathrm{D}^d + \mathrm{p}^d + \overline{\mathrm{p}}^d + \mathrm{q}^d + \overline{\mathrm{q}}^d + \mathrm{r}^d + \overline{\mathrm{r}}^d + \mathrm{s}^d + \overline{\mathrm{s}}^d \tag{17}$$

By introducing the ligand-inventory functions (Eq. 17) into the CI-CF($\boldsymbol{C}_2, b_d$) (`CICF_C2`) shown in Table 2, we are able to conduct enumeration under the point group $\boldsymbol{C}_2$. In a similar way, the introduction of the ligand-inventory functions (Eqs. 15–17) into the CI-CF($\boldsymbol{C}_{2v}, \$_d$) (`CICF_C2v`) shown in Table 2 enable us to conduct enumeration under the point group $\boldsymbol{C}_{2v}$.

The enumerations using the ligand-inventory functions (Eqs. 15–17) differentiate two chiral ligands (or proligands) of a single enantiomeric pair (i.e., p vs. $\overline{\mathrm{p}}$ etc.), so that two modes of packing for such chiral (pro)ligands are considered in the case of an enantiospheric cycle (cf. the ligand-inventory function for c_d, Eq. 16) as well as in the case of a hemispheric cycle (cf. the ligand-inventory function for b_d, Eq. 17). Suppose that such pairwise chiral (pro)ligands (i.e., p vs. $\overline{\mathrm{p}}$ etc.) are bundled into a single species, i.e., $\ddot{\mathrm{p}}$ etc., whereas such two modes of packing are maintained, or in other words, (pro)ligands are considered to be 3D structures. This means that the ligand-inventory functions (Eqs. 15–17) are transformed into the following ligand-inventory functions for 3D enumeration:

$$a_d = \mathrm{A}^d + \mathrm{B}^d + \mathrm{C}^d + \mathrm{D}^d \tag{18}$$

$$c_d = \mathrm{A}^d + \mathrm{B}^d + \mathrm{C}^d + \mathrm{D}^d + 2\ddot{\mathrm{p}}^d + 2\ddot{\mathrm{q}}^d + 2\ddot{\mathrm{r}}^d + 2\ddot{\mathrm{s}}^d \tag{19}$$

$$b_d = \mathrm{A}^d + \mathrm{B}^d + \mathrm{C}^d + \mathrm{D}^d + 2\ddot{\mathrm{p}}^d + 2\ddot{\mathrm{q}}^d + 2\ddot{\mathrm{r}}^d + 2\ddot{\mathrm{s}}^d, \tag{20}$$

3.2.2 Calculation of generating functions for 3D enumeration

By introducing the ligand-inventory function (Eq. 20) into the CI-CF($\boldsymbol{C}_2, b_d$) (`CICF_C2`) shown in Table 2, we are able to conduct enumeration under the point group $\boldsymbol{C}_2$. The following generating function is obtained:

$$\sum_{\theta} T_{(\boldsymbol{C}_2)\ddot{\theta}} W_{\ddot{\theta}} = \text{CI-CF}(\boldsymbol{C}_2, b_d)\Bigg|_{\text{Eq. 20}}, \tag{21}$$

where the coefficient $T_{(\boldsymbol{C}_2)\ddot{\theta}}$ of the weight $W_{\ddot{\theta}}$ indicates the number of oxirane derivatives with the composition $W_{\ddot{\theta}}$, which are inequivalent with each other under the point group

$\boldsymbol{C}_2$. Thus, each chiral oxirane derivative of enantiomeric pairs (and each achiral oxirane derivative) is counted once during this enumeration. The weight $W_{\ddot{\theta}}$ is represented by the symbol $\mathrm{A}^a\mathrm{B}^b\mathrm{C}^c\mathrm{D}^d\ddot{\mathrm{p}}^{\ddot{p}}\ddot{\mathrm{q}}^{\ddot{q}}\ddot{\mathrm{r}}^{\ddot{r}}\ddot{\mathrm{s}}^{\ddot{s}}$, where $\ddot{\theta}$ represents the following partition:

$$\ddot{\theta} = [a, b, c, d, \ddot{p}, \ddot{q}, \ddot{r}, \ddot{s}], \tag{22}$$

which satisfies

$$a + b + c + d + \ddot{p} + \ddot{q} + \ddot{r} + \ddot{s} = 4. \tag{23}$$

Because the terms in the generating functions appear symmetrically, the partition $\ddot{\theta}$ (Eq. 22) can be regarded as satisfying $a \geq b \geq c \geq d$; and $\ddot{p} \geq \ddot{q} \geq \ddot{r} \geq \ddot{s}$.

The coefficient $T_{(\boldsymbol{C}_2)\ddot{\theta}}$ of each weight $W_{\ddot{\theta}}$ in the generating function (Eq. 21) is listed in the $T_{(\boldsymbol{C}_2)\ddot{\theta}}$-column of Table 3. The results of Table 3 are consistent with the data of Table 12 of [21], which is based on an alternative formulation other than combined-permutation representations.

Table 3. Hierarchical Enumeration of Oxirane Derivatives

partition		numbers of oxirane derivatives under respective groups				
		$T_{(\boldsymbol{C}_2)\ddot{\theta}}$	$B_{(\boldsymbol{C}_{2v})\ddot{\theta}}$	$B_{(\boldsymbol{C}_{2v\widetilde{\sigma}\widehat{I}})\ddot{\theta}}$	$B_{(\widetilde{\boldsymbol{C}}_{2v\widetilde{\sigma}\widehat{I}})\ddot{\theta}}$	$B_{(\widetilde{\widetilde{\boldsymbol{C}}}_{2v\widetilde{\sigma}\widehat{I}})\ddot{\theta}}$
		(Eq. 21)	(Eq. 24)	(Eq. 25)	(Eq. 28)	(Eq. 29)
		Eqs. 18–20			Eq. 27	
$[\ddot{\theta}]_1 =$	$[4,0,0,0,0,0,0,0]$	1	1	1	1	1
$[\ddot{\theta}]_2 =$	$[3,1,0,0,0,0,0,0]$	2	1	1	1	1
$[\ddot{\theta}]_3 =$	$[3,0,0,0,1,0,0,0]$	4	2	1	1	1
$[\ddot{\theta}]_4 =$	$[2,2,0,0,0,0,0,0]$	4	3	3	2	1
$[\ddot{\theta}]_5 =$	$[2,0,0,0,2,0,0,0]$	14	9	6	2	1
$[\ddot{\theta}]_6 =$	$[2,1,1,0,0,0,0,0]$	6	3	3	2	1
$[\ddot{\theta}]_7 =$	$[2,1,0,0,1,0,0,0]$	12	6	3	2	1
$[\ddot{\theta}]_8 =$	$[2,0,0,0,1,1,0,0]$	24	12	6	2	1
$[\ddot{\theta}]_9 =$	$[1,1,1,1,0,0,0,0]$	12	6	6	3	1
$[\ddot{\theta}]_{10} =$	$[1,1,1,0,1,0,0,0]$	24	12	6	3	1
$[\ddot{\theta}]_{11} =$	$[1,1,0,0,2,0,0,0]$	24	12	6	2	1
$[\ddot{\theta}]_{12} =$	$[1,1,0,0,1,1,0,0]$	48	24	12	3	1
$[\ddot{\theta}]_{13} =$	$[1,0,0,0,3,0,0,0]$	16	8	4	1	1
$[\ddot{\theta}]_{14} =$	$[1,0,0,0,2,1,0,0]$	48	24	12	2	1
$[\ddot{\theta}]_{15} =$	$[1,0,0,0,1,1,1,0]$	96	48	24	3	1
$[\ddot{\theta}]_{16} =$	$[0,0,0,0,4,0,0,0]$	10	7	5	1	1
$[\ddot{\theta}]_{17} =$	$[0,0,0,0,3,1,0,0]$	32	16	8	1	1
$[\ddot{\theta}]_{18} =$	$[0,0,0,0,2,2,0,0]$	52	30	18	2	1
$[\ddot{\theta}]_{19} =$	$[0,0,0,0,2,1,1,0]$	96	48	24	2	1
$[\ddot{\theta}]_{20} =$	$[0,0,0,0,1,1,1,1]$	192	96	48	3	1

On the other hand, the introduction of the ligand-inventory functions (Eqs. 18–20) into the CI-CF($\boldsymbol{C}_{2v}, \$_d$) (`CICF_C2v`) shown in Table 2 enable us to conduct enumeration under the point group $\boldsymbol{C}_{2v}$ in the form of the following generating function:

$$\sum_{\theta} B_{(\boldsymbol{C}_{2v})\ddot{\theta}} W_{\ddot{\theta}} = \text{CI-CF}(\boldsymbol{C}_{2v}, \$_d)\Bigg|_{\text{Eqs. 18–20}}, \tag{24}$$

where the coefficient $B_{(\boldsymbol{C}_{2v})\ddot{\theta}}$ of the weight $W_{\ddot{\theta}}$ indicates the number of pairs of enantiomeric oxirane derivatives with the composition $W_{\ddot{\theta}}$, which are inequivalent with each other under the point group $\boldsymbol{C}_{2v}$. Thus, each pair of (self-)enantiomeric oxirane derivatives is counted once under this enumeration. The coefficient $B_{(\boldsymbol{C}_{2v})\ddot{\theta}}$ of each weight $W_{\ddot{\theta}}$ in the generating function (Eq. 24) is listed in the $B_{(\boldsymbol{C}_{2v})\ddot{\theta}}$-column of Table 3.

The above-mentioned procedure for the point groups $\boldsymbol{C}_2$ and $\boldsymbol{C}_{2v}$ can be extended to the enumeration under the *RS*-stereoisomeric group $\boldsymbol{C}_{2v\widetilde{\sigma}\widehat{I}}$. Thus, the ligand-inventory functions (Eqs. 18–20) are introduced into CI-CF($\boldsymbol{C}_{2v\widetilde{\sigma}\widehat{I}}, \$_d$) (`CICF_C2vsI`) shown in Table 2, so as to give the following generating function:

$$\sum_{\theta} B_{(\boldsymbol{C}_{2v\widetilde{\sigma}\widehat{I}})\ddot{\theta}} W_{\ddot{\theta}} = \text{CI-CF}(\boldsymbol{C}_{2v\widetilde{\sigma}\widehat{I}}, \$_d)\Bigg|_{\text{Eqs. 18–20}}, \tag{25}$$

where the coefficient $B_{(\boldsymbol{C}_{2v\widetilde{\sigma}\widehat{I}})\ddot{\theta}}$ of the weight $W_{\ddot{\theta}}$ indicates the number of quadruplets of *RS*-stereoisomeric oxirane derivatives with the composition $W_{\ddot{\theta}}$, which are inequivalent with each other under the *RS*-stereoisomeric group $\boldsymbol{C}_{2v\widetilde{\sigma}\widehat{I}}$. Thus, each quadruplet of *RS*-stereoisomeric oxirane derivatives is counted once under this enumeration. The coefficient $B_{(\boldsymbol{C}_{2v\widetilde{\sigma}\widehat{I}})\ddot{\theta}}$ of each weight $W_{\ddot{\theta}}$ in the generating function (Eq. 25) is listed in the $B_{(\boldsymbol{C}_{2v\widetilde{\sigma}\widehat{I}})\ddot{\theta}}$-column of Table 3.

3.3 Enumerations under the stereoisomeric group and under the isoskeletal group

3.3.1 A single ligand–inventory function for stereoisomeric groups and isoskeletal groups

In order to discuss stereoisomers and isoskeletomers, two enantiomeric (pro)ligands in isolation, i.e., p/$\overline{\mathrm{p}}$, q/$\overline{\mathrm{q}}$, r/$\overline{\mathrm{r}}$, or s/$\overline{\mathrm{s}}$, are considered to coincide into a single graph, i.e., $\ddot{\mathrm{p}}$, $\ddot{\mathrm{q}}$, $\ddot{\mathrm{r}}$, or $\ddot{\mathrm{s}}$. Thereby, the ligand inventory $\boldsymbol{L}$ (Eq. 14) is transformed into the following ligand inventory for graph enumeration:

$$\boldsymbol{L}' = \{\mathrm{A}, \mathrm{B}, \mathrm{C}, \mathrm{D}; \ddot{\mathrm{p}}, \ddot{\mathrm{q}}, \ddot{\mathrm{r}}, \ddot{\mathrm{s}}\}, \tag{26}$$

where the uppercase letters A, B, C, and D represent achiral proligands, while the symbols $\ddot{\mathrm{p}}$, $\ddot{\mathrm{q}}$, $\ddot{\mathrm{r}}$, and $\ddot{\mathrm{s}}$ represent graphs generated from p/$\overline{\mathrm{p}}$, q/$\overline{\mathrm{q}}$, r/$\overline{\mathrm{r}}$, and s/$\overline{\mathrm{s}}$.

Suppose that four proligands are selected from the ligand inventory $\boldsymbol{L}'$ (Eq. 26) and placed on the four positions of the oxirane skeleton (**1**), which are considered to be controlled by the stereoisomeric group $\widetilde{\boldsymbol{C}}_{2v\widetilde{\sigma}\widehat{I}}$ or the isoskeletal group $\widetilde{\widetilde{\boldsymbol{C}}}_{2v\widetilde{\sigma}\widehat{I}}$. Then the following ligand-inventory function for graph enumeration is obtained as a degenerate expression:

$$a_d = c_d = b_d = \mathrm{A}^d + \mathrm{B}^d + \mathrm{C}^d + \mathrm{D}^d + \ddot{\mathrm{p}}^d + \ddot{\mathrm{q}}^d + \ddot{\mathrm{r}}^d + \ddot{\mathrm{s}}^d, \tag{27}$$

where both achiral proligands (A, B, C, and D) and chiral proligands ($\ddot{\mathrm{p}}$, $\ddot{\mathrm{q}}$, $\ddot{\mathrm{r}}$, and $\ddot{\mathrm{s}}$) are regarded as graphs (2D structures), so that their behaviors are not differentiated during graph enumeration for counting stereoisomers and isoskeletomers.

3.3.2 Calculation of generating functions for graph enumeration

The ligand-inventory function (Eq. 27) is introduced into CI-CF($\widetilde{\boldsymbol{C}}_{2v\widetilde{\sigma}\widehat{I}}, \$_d$) (`CICF_cC2vsI`) shown in Table 2, so as to give the following generating function:

$$\sum_{\theta} B_{(\widetilde{\boldsymbol{C}}_{2v\widetilde{\sigma}\widehat{I}})\ddot{\theta}} W_{\ddot{\theta}} = \text{CI-CF}(\widetilde{\boldsymbol{C}}_{2v\widetilde{\sigma}\widehat{I}}, \$_d)\Big|_{\text{Eq. 27}}, \tag{28}$$

where the coefficient $B_{(\widetilde{\boldsymbol{C}}_{2v\widetilde{\sigma}\widehat{I}})\ddot{\theta}}$ of the weight $W_{\ddot{\theta}}$ indicates the number of sets of stereoisomeric oxirane derivatives with the composition $W_{\ddot{\theta}}$, which are inequivalent with each other under the stereoisomeric group $\widetilde{\boldsymbol{C}}_{2v\widetilde{\sigma}\widehat{I}}$. Thus, each set of stereoisomeric oxirane derivatives is counted once under this enumeration. The coefficient $B_{(\widetilde{\boldsymbol{C}}_{2v\widetilde{\sigma}\widehat{I}})\ddot{\theta}}$ of each weight $W_{\ddot{\theta}}$ in the generating function (Eq. 28) is listed in the $B_{(\widetilde{\boldsymbol{C}}_{2v\widetilde{\sigma}\widehat{I}})\ddot{\theta}}$-column of Table 3.

On the other hand, we obtain the following generating function by introducing the ligand-inventory function (Eq. 27) into CI-CF($\widetilde{\widetilde{\boldsymbol{C}}}_{2v\widetilde{\sigma}\widehat{I}}, \$_d$) (`CICF_ccC2vsI`):

$$\sum_{\theta} B_{(\widetilde{\widetilde{\boldsymbol{C}}}_{2v\widetilde{\sigma}\widehat{I}})\ddot{\theta}} W_{\ddot{\theta}} = \text{CI-CF}(\widetilde{\widetilde{\boldsymbol{C}}}_{2v\widetilde{\sigma}\widehat{I}}, \$_d)\Big|_{\text{Eq. 27}}, \tag{29}$$

where the coefficient $B_{(\widetilde{\widetilde{\boldsymbol{C}}}_{2v\widetilde{\sigma}\widehat{I}})\ddot{\theta}}$ of the weight $W_{\ddot{\theta}}$ indicates the number of sets of isoskeletomeric oxirane derivatives with the composition $W_{\ddot{\theta}}$, which are inequivalent with each other under the isoskeletal group $\widetilde{\widetilde{\boldsymbol{C}}}_{2v\widetilde{\sigma}\widehat{I}}$. Thus, each set of isoskeletomeric oxirane derivatives is counted once under this enumeration. The coefficient $B_{(\widetilde{\widetilde{\boldsymbol{C}}}_{2v\widetilde{\sigma}\widehat{I}})\ddot{\theta}}$ of each weight $W_{\ddot{\theta}}$ in the generating function (Eq. 29) is listed in the $B_{(\widetilde{\widetilde{\boldsymbol{C}}}_{2v\widetilde{\sigma}\widehat{I}})\ddot{\theta}}$-column of Table 3, which exhibits the presence of a single set of isoskeletomers.

4 Isomer–classification diagrams for testifying enumeration results

4.1 Oxirane derivatives with the composition $\mathrm{A}^2\mathrm{B}^2$

To confirm the validity of the enumeration results collected in Table 3, let us first examine the $[\ddot{\theta}]_4$-row concerning oxirane derivatives with the composition $\mathrm{A}^2\mathrm{B}^2$. This derivation is conducted by placing the set of proligands $\mathrm{A}^2\mathrm{B}^2$ on the four positions of the numbered skeleton **1** (Figure 2) according to the following function:

$$f_1 : f_1(1) = \mathrm{A}, f_1(2) = \mathrm{B}, f_1(3) = \mathrm{B}, f_1(4) = \mathrm{A}, \tag{30}$$

where the function f_1 means the placement of A on the position 1, and so on. Thereby, the 24 modes of permutations shown in Figure 2 generate possible derivatives, which may coincide to give degenerate promolecules, as shown in Figure 3. This figure is cited from [29] (Figure 18) after modification. Note that each quadruplet contained in Figure 2 generates a stereoisogram governed by the RS-stereoisomeric group $\boldsymbol{C}_{2v\widetilde{\sigma}\widehat{I}}$, as shown in Figure 3, where the specification of type $(\text{I–IV})^2/\text{IV}^2$ depends on the modes of degeneration [29]. Note that the the RS-stereoisomeric group $\boldsymbol{C}_{2v\widetilde{\sigma}\widehat{I}}$ is a normal subgroup of the isoskeletal group $\widetilde{\widetilde{\boldsymbol{C}}}_{2v\widetilde{\sigma}\widehat{I}}$), as confirmed by inputting the following commands:

```
gap> C2vsI := Group([ (5,6), (1,2)(3,4), (1,3)(2,4) ]);
Group([ (5,6), (1,2)(3,4), (1,3)(2,4) ])
gap> ccC2vsI := Group([ (5,6), (3,4), (2,3), (1,2) ]);
Group([ (5,6), (3,4), (2,3), (1,2) ])
gap> ConjugateSubgroups(ccC2vsI, C2vsI);
[ Group([ (5,6), (1,2)(3,4), (1,3)(2,4) ]) ]
gap> IsNormal(ccC2vsI, C2vsI);
true
```

As found by Figure 3, there appear one type-I stereoisogram and two type-IV stereoisograms. The values listed in the $[\ddot{\theta}]_4$-row of Table 3 are confirmed by referring to Figure 3. The value $T_{(\boldsymbol{C}_2)[\ddot{\theta}]_4} = 4$ indicates the presence of four promolecules under the action of the point group $\boldsymbol{C}_2$, so that **14**, $\overline{\mathbf{14}}$, **16**, and **18** are inequivalent to each other to be counted separately under $\boldsymbol{C}_2$. The value $B_{(\boldsymbol{C}_{2v})[\ddot{\theta}]_4} = 3$ indicates the presence of three pairs of (self-)enantiomers under the action of the point group $\boldsymbol{C}_{2v}$, so that one pair of enantiomers [**14** $\overline{\mathbf{14}}$], one achiral promolecule [**16**], and one achiral promolecule [**18**] are equivalence classes, which are inequivalent (i.e., diastereomeric) to each other to be counted separately under $\boldsymbol{C}_{2v}$. The value $B_{(\boldsymbol{C}_{2v\widetilde{\sigma}\widehat{I}})[\ddot{\theta}]_4} = 3$ indicates the presence of three quadruplets of RS-stereoisomers under the action of the RS-stereoisomeric group $\boldsymbol{C}_{2v\widetilde{\sigma}\widehat{I}}$. Thus, one type-I stereoisogram containing a pair of enantiomers ([**14** $\overline{\mathbf{14}}$])$_{\mathrm{I}}$, one type-IV stereoisogram containing ([**16**])$_{\mathrm{IV}}$, and one type-IV stereoisogram containing ([**18**])$_{\mathrm{IV}}$ exhibit respective quadruplets as equivalence classes, which are inequivalent to be counted separately under $\boldsymbol{C}_{2v\widetilde{\sigma}\widehat{I}}$. The value $B_{(\widetilde{\boldsymbol{C}}_{2v\widetilde{\sigma}\widehat{I}})[\ddot{\theta}]_4} = 2$ indicates the presence of two sets

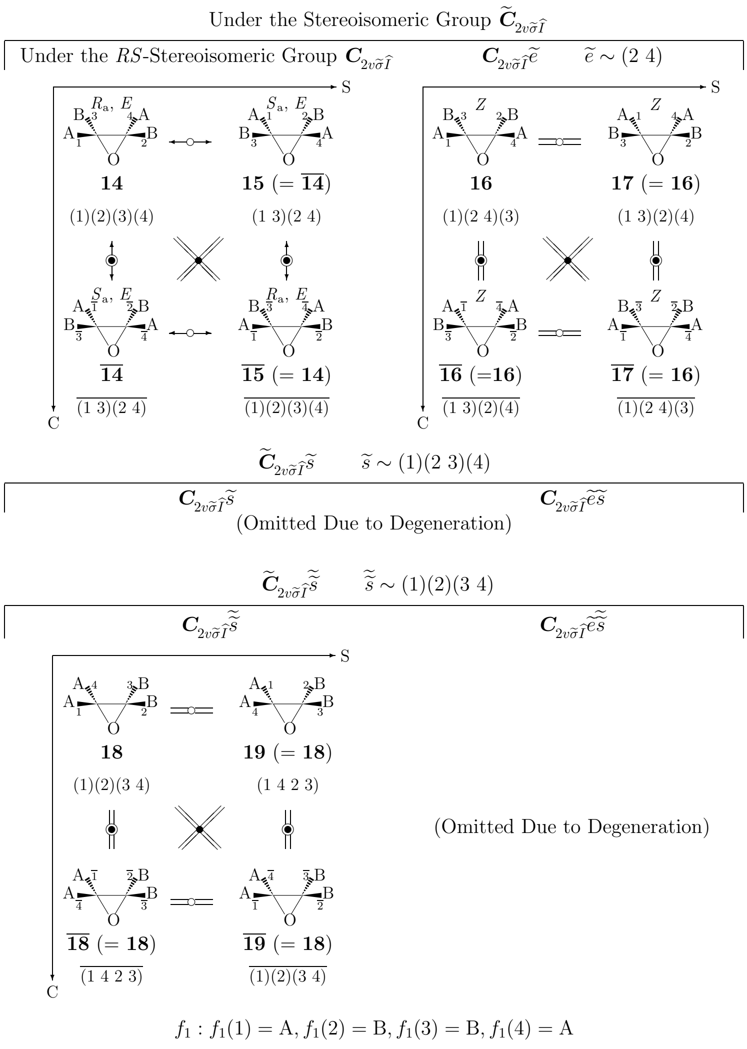

Figure 3. Hierarchy diagram for representing a multiple stereoisogram set of type $(\text{I–IV})^2/\text{IV}^2$ derived from the oxirane skeleton **1**, where the substitution function f_1 is applied to Fig. 2. Note that the uppercase letters A and B represent achiral proligands in isolation, where the priority sequence is presumed to be A > B. Figure 18 of [29] is cited after modification.

of stereoisomers under the action of the stereoisomeric group $\widetilde{\boldsymbol{C}}_{2v\widetilde{\sigma}\widehat{I}}$, so that one set of stereoisomers $\langle([\mathbf{14}\ \overline{\mathbf{14}}])_{\mathrm{I}}\ ([\mathbf{16}])_{\mathrm{IV}}\rangle$ (one pair of enantiomers $\mathbf{14}/\overline{\mathbf{14}}$ and one achiral promolecule **16**) and one set of self-stereoisomers $\langle([\mathbf{16}])_{\mathrm{I}}\rangle$ (one single-membered set of an achiral promolecule **16**) are equivalence classes, which are inequivalent (i.e., constitutionally anisomeric) to each other to be counted separately under $\widetilde{\boldsymbol{C}}_{2v\widetilde{\sigma}\widehat{I}}$. Finally, the value $B_{(\widetilde{\widetilde{\boldsymbol{C}}}_{2v\widetilde{\sigma}\widehat{I}})[\ddot{\theta}]_4} = 1$ indicates the presence of one set of isoskeletomers, which is recognized as an equivalence class to be counted once under the action of the isoskeletal group $\widetilde{\widetilde{\boldsymbol{C}}}_{2v\widetilde{\sigma}\widehat{I}}$.

The modes of enumeration described in the preceding paragraph can be schematically expressed by the following *isomer-classification scheme*:

$$\left\{\left\langle([\mathbf{14}\ \overline{\mathbf{14}}])_{\mathrm{I}}\ ([\mathbf{16}])_{\mathrm{IV}}\right\rangle \left\langle([\mathbf{18}])_{\mathrm{IV}}\right\rangle\right\}, \tag{31}$$

where a pair of square brackets contains a pair of (self-)enantiomers (totally three pairs of square brackets, $B_{(\boldsymbol{C}_{2v})[\ddot{\theta}]_4} = 3$), a pair of parentheses contains a quadruplet of RS-stereoisomers (totally three pairs of parentheses, $B_{(\boldsymbol{C}_{2v\widetilde{\sigma}\widehat{I}})[\ddot{\theta}]_4} = 3$), a pair of angle brackets contains an equivalence class of stereoisomers (totally two pairs of angle brackets, $B_{(\widetilde{\boldsymbol{C}}_{2v\widetilde{\sigma}\widehat{I}})[\ddot{\theta}]_4} = 2$), and a pair of braces contains an equivalence class of isoskeletomers (totally one pair of braces, $B_{(\widetilde{\widetilde{\boldsymbol{C}}}_{2v\widetilde{\sigma}\widehat{I}})[\ddot{\theta}]_4} = 1$). Note that a pair of parentheses is attached by a Roman numeral (I–V) as a subscript to show the type of the stereoisogram at issue.

For the sake of simplicity, the combination of an hierarchy diagram (e.g., Figure 3) and an isomer-classification scheme (e.g., Eq. 31) can be replaced by an *isomer-classification diagram* [10]. Figure 4 shows an *isomer-classification diagram* corresponding to the combination of Figure 3 and Eq. 31. This isomer-classification diagram clarifies the rationality of the hierarchy represented by Eqs.1–3.

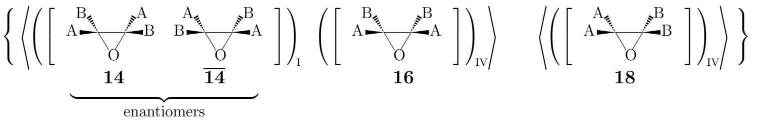

Figure 4. Isomer-classification diagram for oxiranes with the composition A^2B^2. A pair of square brackets contains a pair of (self)-enantiomers, a pair of parentheses contains a quadruplet of RS-stereoisomers, a pair of angles contains an equivalence class of stereoisomers, and a pair of braces contains an equivalence class of isoskeletomers.

4.2 Oxirane derivatives with the composition ABCD

Let us next examine the $[\ddot{\theta}]_9$-row concerning oxirane derivatives with the composition ABCD, which are generated by applying the following function:

$$f_2 : f_2(1) = \mathrm{A}, f_2(2) = \mathrm{C}, f_2(3) = \mathrm{B}, f_2(4) = \mathrm{D}. \tag{32}$$

to the four positions of the numbered skeleton **1** (Figure 2). Thereby, the 24 modes of permutations shown in Figure 2 generate possible derivatives. In a similar way to the procedure described in the preceding subsection, the corresponding isomer-classification diagram is obtained, as shown in Figure 5, which is cited from [10] (Figure 9) after modification and the correction of numbering.

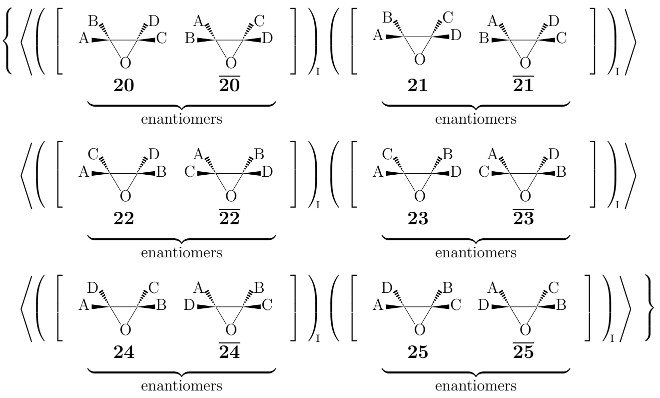

Figure 5. Isomer-classification diagram for oxirane derivatives with the composition ABCD. This figure is cited from [10] (Figure 9) after modification.

By referring to Figure 5, let us examine the values listed in the $[\ddot{\theta}]_9$-row of Table 3. The value $T_{(\boldsymbol{C}_2)[\ddot{\theta}]_9} = 12$ indicates the presence of twelve promolecules under the action of the point group $\boldsymbol{C}_2$. These correspond to the twelve chiral promolecules (**20**, $\overline{\mathbf{20}}$, **21**, $\overline{\mathbf{21}}$, $\cdots$, **25**, $\overline{\mathbf{25}}$) depicted in Figure 5, which are inequivalent to each other to be counted separately under $\boldsymbol{C}_2$. The value $B_{(\boldsymbol{C}_{2v})[\ddot{\theta}]_9} = 6$ indicates the presence of six pairs of enantiomers under the action of the point group $\boldsymbol{C}_{2v}$. As depicted in Figure 5, each of these pairs is surrounded by a pair of square brackets, e.g., [**20** $\overline{\mathbf{20}}$], which is counted once as an equivalence class under $\boldsymbol{C}_{2v}$. The value $B_{(\boldsymbol{C}_{2v\widetilde{\sigma}\widehat{I}})[\ddot{\theta}]_9} = 6$ indicates the presence of six quadruplets of RS-stereoisomers under the action of the RS-stereoisomeric group $\boldsymbol{C}_{2v\widetilde{\sigma}\widehat{I}}$. Thus, each of these quadruplets degenerates into a pair of enantiomers, e.g., ([**20** $\overline{\mathbf{20}}$])$_{\mathrm{I}}$, which is counted once as an equivalence class under $\boldsymbol{C}_{2v\widetilde{\sigma}\widehat{I}}$. The value $B_{(\widetilde{\boldsymbol{C}}_{2v\widetilde{\sigma}\widehat{I}})[\ddot{\theta}]_9} = 3$

indicates the presence of three equivalence classes of stereoisomers under the action of the stereoisomeric group $\widetilde{\boldsymbol{C}}_{2v\widetilde{\sigma}\widehat{I}}$. Each of these equivalence classes is surrounded by a pair of angle brackets, e.g., $\langle([\mathbf{20}\ \overline{\mathbf{20}}])_{\mathrm{I}}\ ([\mathbf{21}\ \overline{\mathbf{21}}])_{\mathrm{I}}\rangle$, which is counted once as an equivalence class (due to *cis/trans*-isomerism) under $\widetilde{\boldsymbol{C}}_{2v\widetilde{\sigma}\widehat{I}}$. Finally, the value $B_{(\widetilde{\widetilde{\boldsymbol{C}}}_{2v\widetilde{\sigma}\widehat{I}})[\ddot{\theta}]_9} = 1$ indicates the presence of one set of isoskeletomers, which is recognized as an equivalence class to be counted once under the action of the isoskeletal group $\widetilde{\widetilde{\boldsymbol{C}}}_{2v\widetilde{\sigma}\widehat{I}}$.

4.3 Oxirane derivatives with the compositions $\mathbf{A}^2\mathbf{p}\overline{\mathbf{p}}$ and $\mathbf{A}^2\mathbf{p}^2$ (or $\mathbf{A}^2\overline{\mathbf{p}}^2$)

To demonstrate the effects of chiral proligands, let us examine the $[\ddot{\theta}]_5$-row of Table 3, which corresponds to the compositions $\mathrm{A}^2\mathrm{p}\overline{\mathrm{p}}$ and $\mathrm{A}^2\mathrm{p}^2$ (or $\mathrm{A}^2\overline{\mathrm{p}}^2$). To solve this examination, a function for the composition the compositions $\mathrm{A}^2\mathrm{p}\overline{\mathrm{p}}$:

$$f_3 : f_3(1) = \mathrm{A}, f_3(2) = \mathrm{A}, f_3(3) = \mathrm{p}, f_3(4) = \overline{\mathrm{p}} \tag{33}$$

and another function for the composition $\mathrm{A}^2\mathrm{p}^2$ (or $\mathrm{A}^2\overline{\mathrm{p}}^2$):

$$f_4 : f_4(1) = \mathrm{A}, f_4(2) = \mathrm{A}, f_4(3) = \mathrm{p}, f_4(4) = \mathrm{p} \tag{34}$$

should be considered to consider the ligand-inventory functions represented by Eqs. 18–20. According to the first function, a set of 24 modes of permutations shown in Figure 2 generate possible derivatives with the composition $\mathrm{A}^2\mathrm{p}\overline{\mathrm{p}}$, while another set of 24 modes of permutations shown in Figure 2 generate possible derivatives with the composition $\mathrm{A}^2\mathrm{p}^2$ (or $\mathrm{A}^2\overline{\mathrm{p}}^2$). In contrast, the degenerate ligand-inventory function (Eq. 27) requires the following degenerate function:

$$f_3' : f_3'(1) = \mathrm{A}, f_3'(2) = \mathrm{A}, f_3'(3) = \ddot{\mathrm{p}}, f_3'(4) = \ddot{\mathrm{p}}. \tag{35}$$

These functions are applied to the four positions of the numbered skeleton **1** (Figure 2) according to the purposes of enumeration. The results should be compared with one another to comprehend the isomer hierarchy characterized by the $[\ddot{\theta}]_5$-row of Table 3. Figure 6 shows an isomer-classification diagram corresponding to the $[\ddot{\theta}]_5$-row of Table 3, which lists the numbers of oxirane derivatives with the compositions $\mathrm{A}^2\mathrm{p}\overline{\mathrm{p}}$ and $\mathrm{A}^2\mathrm{p}^2$ (or $\mathrm{A}^2\overline{\mathrm{p}}^2$). Let us examine the values listed in the $[\ddot{\theta}]_5$-row of Table 3 by referring to the isomer-classification diagram (Figure 6).

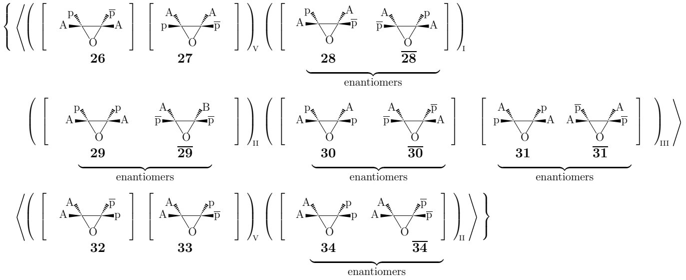

Figure 6. Isomer-classification diagram for oxirane derivatives with the compositions $\mathrm{A}^2\mathrm{p}\overline{\mathrm{p}}$ and $\mathrm{A}^2\mathrm{p}^2$ (or $\mathrm{A}^2\overline{\mathrm{p}}^2$).

The value $T_{(\boldsymbol{C}_2)[\ddot{\theta}]_5} = 14$ appearing in the $[\ddot{\theta}]_5$-row of Table 3 indicates the presence of fourteen promolecules under the action of the point group $\boldsymbol{C}_2$. These correspond to the four achiral promolecules (**26**, **27**, **32**, and **33**) and the ten chiral promolecules (**28**, $\overline{\mathbf{28}}$, etc.) depicted in Figure 6. Note that each promolecule is counted once as a molecular entity under the action of the point group $\boldsymbol{C}_2$.

The value $B_{(\boldsymbol{C}_{2v})[\ddot{\theta}]_5} = 9$ indicates the presence of nine pairs of (self-)enantiomers under the action of the point group $\boldsymbol{C}_{2v}$. As surrounded by pairs of square brackets, there appear four achiral promolecules ([**26**], [**27**], [**32**], and [**33**] as pairs of self-enantiomers) and five pairs of enantiomers (e.g., [**28** $\overline{\mathbf{28}}$] and [**29** $\overline{\mathbf{29}}$]). Each pair of (self-)enantiomers is counted once as an equivalence class under $\boldsymbol{C}_{2v}$.

The value $B_{(\boldsymbol{C}_{2v\widetilde{\sigma}\widehat{I}})[\ddot{\theta}]_5} = 6$ indicates the presence of six quadruplets of RS-stereoisomers under the action of the RS-stereoisomeric group $\boldsymbol{C}_{2v\widetilde{\sigma}\widehat{I}}$, as enclosed by six pairs of parentheses. Each of these quadruplets is characterized by a stereoisogram, the type (I, II, III, or V) of which is shown as a subscript attached to a closing parenthesis. Note that a type-V quadruplet degenerates into two achiral promolecules (e.g., $([\mathbf{26}], [\mathbf{27}])_{\mathrm{V}}$); a type-I quadruplet degenerates into a pair of enantiomers (e.g., $([\mathbf{28}\ \overline{\mathbf{28}}])_{\mathrm{I}}$); and a type-II quadruplet degenerates into a pair of enantiomers (e.g., $([\mathbf{29}\ \overline{\mathbf{29}}])_{\mathrm{II}}$). In contrast, a type-III quadruplet exhibits no degeneration, e.g., $([\mathbf{30}\ \overline{\mathbf{30}}]\ [\mathbf{31}\ \overline{\mathbf{31}}])_{\mathrm{III}}$.

The value $B_{(\widetilde{\boldsymbol{C}}_{2v\widetilde{\sigma}\widehat{I}})[\ddot{\theta}]_5} = 2$ indicates the presence of two equivalence classes of stereoisomers under the action of the stereoisomeric group $\widetilde{\boldsymbol{C}}_{2v\widetilde{\sigma}\widehat{I}}$, as surrounded by two pairs of angle brackets in Figure 6.

Finally, the value $B_{(\widetilde{\widetilde{\boldsymbol{C}}}_{2v\widetilde{\sigma}\widehat{I}})[\ddot{\theta}]_5} = 1$ indicates the presence of one set of isoskeletomers, which is surrounded by a pair of braces. This set is recognized as an equivalence class to be counted once under the action of the isoskeletal group $\widetilde{\widetilde{\boldsymbol{C}}}_{2v\widetilde{\sigma}\widehat{I}}$.

5 *cis/trans*–isomerism vs. stereoisomerism

To compare the usage of the combination of Eqs. 33 and 34 with the usage of Eq. 35, let us try a more general approach from the viewpoint of *cis/trans*-isomerism vs. stereoisomerism.

5.1 Generating functions by considering 3D proligands

The generating functions represented by Eq. 28 and Eq. 29 have been derived by using a single ligand-inventory function (Eq. 27). This means that each proligand is regarded as a graph selected from $\boldsymbol{L}'$ (Eq. 26). To treat proligands as 3D structures in isolation, the ligand-inventory functions represented by Eqs. 18–20 are introduced into the CI-CF under the stereoisomeric group, i.e., CI-CF$(\widetilde{\boldsymbol{C}}_{2v\widetilde{\sigma}\widehat{I}}, \$_d)$.

$$\sum_{\theta} B'_{(\widetilde{\boldsymbol{C}}_{2v\widetilde{\sigma}\widehat{I}})\ddot{\theta}} W_{\ddot{\theta}} = \text{CI-CF}(\widetilde{\boldsymbol{C}}_{2v\widetilde{\sigma}\widehat{I}}, \$_d)\Big|_{\text{Eqs. 18–20}} . \tag{36}$$

The coefficient $B'_{(\widetilde{\boldsymbol{C}}_{2v\widetilde{\sigma}\widehat{I}})\ddot{\theta}}$ of the weight $W_{\ddot{\theta}}$ indicates the number of sets of stereoisomeric oxirane derivatives with the composition $W_{\ddot{\theta}}$, where each proligand is considered to have a 3D structure in isolation. The equivalence under the stereoisomeric group $\widetilde{\boldsymbol{C}}_{2v\widetilde{\sigma}\widehat{I}}$ is judged by taking account of the 3D structure of each proligand. Compare this generating function with the generating function for treating proligands as graphs (Eq. 28), which is based on the single ligand-inventory function (Eq. 27). The coefficients $B'_{(\widetilde{\boldsymbol{C}}_{2v\widetilde{\sigma}\widehat{I}})\ddot{\theta}}$ in Eq. 36 are listed in the corresponding column of Table 4.

In a similar way, the ligand-inventory functions represented by Eqs. 18–20 are introduced into the CI-CF under the isoskeletal group, i.e., CI-CF$(\widetilde{\widetilde{\boldsymbol{C}}}_{2v\widetilde{\sigma}\widehat{I}}, \$_d)$).

$$\sum_{\theta} B'_{(\widetilde{\widetilde{\boldsymbol{C}}}_{2v\widetilde{\sigma}\widehat{I}})\ddot{\theta}} W_{\ddot{\theta}} = \text{CI-CF}(\widetilde{\widetilde{\boldsymbol{C}}}_{2v\widetilde{\sigma}\widehat{I}}, \$_d)\Big|_{\text{Eqs. 18–20}} . \tag{37}$$

The coefficient $B'_{(\widetilde{\widetilde{\boldsymbol{C}}}_{2v\widetilde{\sigma}\widehat{I}})\ddot{\theta}}$ of the weight $W_{\ddot{\theta}}$ in this generating function indicates the number of sets of isoskeletomeric oxirane derivatives with the composition $W_{\ddot{\theta}}$, where each proligand is considered to have a 3D structure in isolation. Again, compare this generating function with the generating function for treating proligands as graphs (Eq. 29), which is based on the single ligand-inventory function (Eq. 27). The coefficients $B'_{(\widetilde{\widetilde{\boldsymbol{C}}}_{2v\widetilde{\sigma}\widehat{I}})\ddot{\theta}}$ in Eq. 37 are listed in the corresponding column of Table 4.

5.2 Proligands as graphs and as 3D structures

The comparison of the data in the two columns of Table 4 with the corresponding data of Table 3 provides us with a quantitative viewpoint concerning *cis/trans*-isomerism vs. stereoisomerism.

Table 4. Stereoisomerism and Isoskeletomerism by Considering 3D Proligands

partition	numbers of oxirane derivatives under respective groups	
	$B'_{(\widetilde{\boldsymbol{C}}_{2v\widetilde{\sigma}\widehat{I}})\ddot{\theta}}$ (Eq. 36)	$B'_{(\widetilde{\widetilde{\boldsymbol{C}}}_{2v\widetilde{\sigma}\widehat{I}})\ddot{\theta}}$ (Eq. 37)
	$\underbrace{\qquad\qquad}_{\text{Eqs. 18–20}}$	
$[\ddot{\theta}]_1 = [4,0,0,0,0,0,0,0]$	1	1
$[\ddot{\theta}]_2 = [3,1,0,0,0,0,0,0]$	1	1
$[\ddot{\theta}]_3 = [3,0,0,0,1,0,0,0]$	1	1
$[\ddot{\theta}]_4 = [2,2,0,0,0,0,0,0]$	2	1
$[\ddot{\theta}]_5 = [2,0,0,0,2,0,0,0]$	4	2
$[\ddot{\theta}]_6 = [2,1,1,0,0,0,0,0]$	2	1
$[\ddot{\theta}]_7 = [2,1,0,0,1,0,0,0]$	2	1
$[\ddot{\theta}]_8 = [2,0,0,0,1,1,0,0]$	4	2
$[\ddot{\theta}]_9 = [1,1,1,1,0,0,0,0]$	3	1
$[\ddot{\theta}]_{10} = [1,1,1,0,1,0,0,0]$	3	1
$[\ddot{\theta}]_{11} = [1,1,0,0,2,0,0,0]$	4	2
$[\ddot{\theta}]_{12} = [1,1,0,0,1,1,0,0]$	6	2
$[\ddot{\theta}]_{13} = [1,0,0,0,3,0,0,0]$	3	2
$[\ddot{\theta}]_{14} = [1,0,0,0,2,1,0,0]$	7	3
$[\ddot{\theta}]_{15} = [1,0,0,0,1,1,1,0]$	12	4
$[\ddot{\theta}]_{16} = [0,0,0,0,4,0,0,0]$	4	3
$[\ddot{\theta}]_{17} = [0,0,0,0,3,1,0,0]$	6	4
$[\ddot{\theta}]_{18} = [0,0,0,0,2,2,0,0]$	11	5
$[\ddot{\theta}]_{19} = [0,0,0,0,2,1,1,0]$	14	6
$[\ddot{\theta}]_{20} = [0,0,0,0,1,1,1,1]$	24	8

When all of the substituents are achiral, the data of $B'_{(\widetilde{\boldsymbol{C}}_{2v\widetilde{\sigma}\widehat{I}})\ddot{\theta}}$-column and $B'_{(\widetilde{\widetilde{\boldsymbol{C}}}_{2v\widetilde{\sigma}\widehat{I}})\ddot{\theta}}$-column in Table 4 are identical with the corresponding data of Table 3, as found in the $[\ddot{\theta}]_1$-rows, the $[\ddot{\theta}]_2$-rows, the $[\ddot{\theta}]_4$-rows, the $[\ddot{\theta}]_6$-rows, and the $[\ddot{\theta}]_9$-rows. As for the $[\ddot{\theta}]_4$-rows, for example, the value $B_{(\widetilde{\boldsymbol{C}}_{2v\widetilde{\sigma}\widehat{I}})[\ddot{\theta}]_4}$ $(= 2)$ is equal to the value $B'_{(\widetilde{\boldsymbol{C}}_{2v\widetilde{\sigma}\widehat{I}})[\ddot{\theta}]_4}$ $(= 2)$, so that each of the two sets of stereoisomers surrounded by pairs of angle brackets (Figure 4) is equal to the corresponding set of *cis/trans*-isomers. A similar discussion is applied to the case of $[\ddot{\theta}]_9$, as shown in the isomer-classification diagram (Figure 5).

When a set of proligands contains only one chiral proligand ($[\ddot{\theta}]_3$, $[\ddot{\theta}]_7$, and $[\ddot{\theta}]_{10}$), the data of the $B'_{(\widetilde{\boldsymbol{C}}_{2v\widetilde{\sigma}\widehat{I}})\ddot{\theta}}$-column and those of the $B'_{(\widetilde{\widetilde{\boldsymbol{C}}}_{2v\widetilde{\sigma}\widehat{I}})\ddot{\theta}}$-column in Table 4 are identical with the corresponding data of Table 3.

The remaining data of Table 4 are different from the corresponding data of Table 3. This means that stereoisomerism (by regarding proligands as graphs) provides equivalence classes different from *cis/trans*-isomerism (by regarding proligands as 3D structures). For example, the value $B_{(\widetilde{\boldsymbol{C}}_{2v\widetilde{\sigma}\widehat{I}})[\ddot{\theta}]_5} = 2$ in Table 3 and the value $B'_{(\widetilde{\boldsymbol{C}}_{2v\widetilde{\sigma}\widehat{I}})[\ddot{\theta}]_5} = 4$ in Table 4 are explained by the following isomer-classification scheme:

$$\begin{gathered} \Big\{\Big\langle \langle\!\bullet ([\mathbf{26}]\ [\mathbf{27}])_{\mathrm{V}}\ ([\mathbf{28}\ \overline{\mathbf{28}}])_{\mathrm{I}} \bullet\!\rangle \\ \langle\!\bullet ([\mathbf{29}\ \overline{\mathbf{29}}])_{\mathrm{II}}\ ([\mathbf{30}\ \overline{\mathbf{30}}]\ [\mathbf{31}\ \overline{\mathbf{31}}])_{\mathrm{III}} \bullet\!\rangle \Big\rangle \\ \Big\langle \langle\!\bullet ([\mathbf{32}]\ [\mathbf{33}])_{\mathrm{V}} \bullet\!\rangle\ \langle\!\bullet ([\mathbf{34}\ \overline{\mathbf{34}}])_{\mathrm{II}} \bullet\!\rangle \Big\rangle \Big\}, \end{gathered} \tag{38}$$

where a pair of angle brackets with bullet symbols, $\langle\!\bullet \cdots \bullet\!\rangle$, represents *cis/trans*-isomerism, which is characterized by the same composition $\mathrm{A}^2\mathrm{p}\overline{\mathrm{p}}$ (or $\mathrm{A}^2\mathrm{p}^2/\mathrm{A}^2\overline{\mathrm{p}}^2$). There appear four sets of *cis/trans*-isomers, where the two sets are contained in a set of stereoisomers $\langle \cdots \rangle$, while the other two sets are contained in another set of stereoisomers $\langle \cdots \rangle$. Thus, Eq. 38 shows that *cis/trans*-isomerism counted by $B'_{(\widetilde{\boldsymbol{C}}_{2v\widetilde{\sigma}\widehat{I}})[\ddot{\theta}]_5}$ (Table 4) can be regarded as a subcategory of stereoisomerism counted by $B_{(\widetilde{\boldsymbol{C}}_{2v\widetilde{\sigma}\widehat{I}})[\ddot{\theta}]_5}$ (Table 3).

Keep in mind the presumption of the present approach that the composition $\mathrm{A}^2\mathrm{p}\overline{\mathrm{p}}$ is differentiated from the composition $\mathrm{A}^2\mathrm{p}^2$ (or $\mathrm{A}^2\overline{\mathrm{p}}^2$) during the recognition of *cis/-trans*-isomerism (Eq. 38). For example, the promolecule **26** with $\mathrm{A}^2\mathrm{p}\overline{\mathrm{p}}$ is not *cis/-trans*-isomeric to the promolecule **30** with $\mathrm{A}^2\mathrm{p}^2$, although they are stereoisomeric to each other. In contrast, the promolecules **26** and **28** having a common composition $\mathrm{A}^2\mathrm{p}\overline{\mathrm{p}}$ are recognized to be *cis/trans*-isomeric to each other (within $\langle\!\bullet \cdots \bullet\!\rangle$), as well as they are stereoisomeric to each other (within $\langle \cdots \rangle$).

On the other hand, the value $B_{(\widetilde{\widetilde{\boldsymbol{C}}}_{2v\widetilde{\sigma}\widehat{I}})[\ddot{\theta}]_5} = 1$ in Table 3 and the value $B'_{(\widetilde{\widetilde{\boldsymbol{C}}}_{2v\widetilde{\sigma}\widehat{I}})[\ddot{\theta}]_5} = 2$ in Table 4 are explained by the following isomer-classification scheme:

$$\begin{gathered} \Big\{ \{\!\bullet \langle\!\bullet ([\mathbf{26}]\ [\mathbf{27}])_{\mathrm{V}}\ ([\mathbf{28}\ \overline{\mathbf{28}}])_{\mathrm{I}} \bullet\!\rangle\ \langle\!\bullet ([\mathbf{32}]\ [\mathbf{33}])_{\mathrm{V}} \bullet\!\rangle \bullet\!\} \\ \{\!\bullet \langle\!\bullet ([\mathbf{29}\ \overline{\mathbf{29}}])_{\mathrm{II}}\ ([\mathbf{30}\ \overline{\mathbf{30}}]\ [\mathbf{31}\ \overline{\mathbf{31}}])_{\mathrm{III}} \bullet\!\rangle\ \langle\!\bullet ([\mathbf{34}\ \overline{\mathbf{34}}])_{\mathrm{II}} \bullet\!\rangle \bullet\!\} \Big\}, \end{gathered} \tag{39}$$

which contains two pairs of braces with bullet symbols $\{\!\bullet \cdots \bullet\!\}$, where each pair of braces with bullet symbols represents a set of isoskeletomers with the same composition $\mathrm{A}^2\mathrm{p}\overline{\mathrm{p}}$ (or $\mathrm{A}^2\mathrm{p}^2/\mathrm{A}^2\overline{\mathrm{p}}^2$). It should be noted that Eq. 39 does not contain pairs of angle brackets, because the scheme is incompatible with stereoisomerism.

It should be emphasized that the stereoisomeric group $\widetilde{\boldsymbol{C}}_{2v\widetilde{\sigma}\widehat{I}}$ (`cC2vsI`) shown in Table 1 can be used in the enumeration of 3D structures (Eq. 36) as well as in the enumeration of graphs (Eq. 28), as shown in the following scheme:

$$\begin{array}{cccc|cc}
\boldsymbol{C}_2 & \boldsymbol{C}_{2v} & \boldsymbol{C}_{2v\widetilde{\sigma}\widehat{I}} & \multicolumn{2}{c}{\overbrace{\hspace{10em}}^{\widetilde{\boldsymbol{C}}_{2v\widetilde{\sigma}\widehat{I}}}} & \widetilde{\widetilde{\boldsymbol{C}}}_{2v\widetilde{\sigma}\widehat{I}} \\
T_{(\boldsymbol{C}_2)\ddot{\theta}} & B_{(\boldsymbol{C}_{2v})\ddot{\theta}} & B_{(\boldsymbol{C}_{2v\widetilde{\sigma}\widehat{I}})\ddot{\theta}} & B'_{(\widetilde{\boldsymbol{C}}_{2v\widetilde{\sigma}\widehat{I}})\ddot{\theta}} & B_{(\widetilde{\boldsymbol{C}}_{2v\widetilde{\sigma}\widehat{I}})\ddot{\theta}} & B_{(\widetilde{\widetilde{\boldsymbol{C}}}_{2v\widetilde{\sigma}\widehat{I}})\ddot{\theta}} \\
(\text{Eq. 21}) & (\text{Eq. 24}) & (\text{Eq. 25}) & (\text{Eq. 36}) & (\text{Eq. 28}) & (\text{Eq. 29}) \\
\multicolumn{4}{c|}{\underbrace{\hspace{24em}}_{\substack{(|_{\text{Eqs. 18–20}}) \\ \text{3D proligands}}}} & \multicolumn{2}{c}{\underbrace{\hspace{10em}}_{\substack{(|_{\text{Eq. 27}}) \\ \text{2D proligands (graphs)}}}}
\end{array} \tag{40}$$

The interface between 3D structures and graphs is evaluated by comparing the $B_{(\widetilde{\boldsymbol{C}}_{2v\widetilde{\sigma}\widehat{I}})\ddot{\theta}}$-column of Table 3 with the $B'_{(\widetilde{\boldsymbol{C}}_{2v\widetilde{\sigma}\widehat{I}})\ddot{\theta}}$-column of Table 4. Compare the isomer-classification diagram (Figure 6) with the scheme represented by Eq. 38 from the viewpoint of *cis/-trans*-isomerism vs. stereoisomerism.

5.3 Correlation to Pólya's theorem

The coefficient $B_{(\widetilde{\boldsymbol{C}}_{2v\widetilde{\sigma}\widehat{I}})\ddot{\theta}}$ of the weight $W_{\ddot{\theta}}$ in Eq. 28 indicates the number of sets of stereoisomeric oxirane derivatives with the composition $W_{\ddot{\theta}}$. The usage of the single ligand-inventory (Eq. 27) means the introduction of $s_d = a_d = c_d = b_d$ into the CI-CF shown in the $\widetilde{\boldsymbol{C}}_{2v\widetilde{\sigma}\widehat{I}}$-part of Table 2, i.e., CI-CF($\widetilde{\boldsymbol{C}}_{2v\widetilde{\sigma}\widehat{I}}, \$_d$) (`CICF_cC2vsI`)). Thereby, the CI-CF degenerates into the following cycle index (CI) without chirality fittingness (CF):

$$\mathrm{CI}(\boldsymbol{G}_{og}, s_d) = \frac{1}{8}s_1^4 + \frac{1}{4}s_1^2 s_2 + \frac{3}{8}s_2^2 + \frac{1}{4}s_4, \tag{41}$$

where the symbol $\boldsymbol{G}_{og}$ represents a permutation group of order 8 for characterizing an oxirane skeleton as a graph. This CI (without CF) is identical with Pólya's cycle index (CI) [32,33], so that the enumeration by Pólya's theorem is regarded as a degenerate case of the present approach based on group hierarchy. The group $\boldsymbol{G}_{og}$ for characterizing an oxirane skeleton as a graph has been discussed briefly in a recent report [34]. Note that $\boldsymbol{G}_{og}$ is generated by starting from a set of generator $[(2,4),(1,2)(3,4)]$ as follows:

```
gap> G_og := Group([ (2,4), (1,2)(3,4) ]);
Group([ (2,4), (1,2)(3,4) ])
gap> Elements(G_og);
[ (), (2,4), (1,2)(3,4), (1,2,3,4), (1,3), (1,3)(2,4),
  (1,4,3,2), (1,4)(2,3) ]
```

The corresponding CI (without CF) is obtained manually by examining the cycle structures of these elements of $\boldsymbol{G}_{og}$, so as to give Eq. 41. Keep in mind, for example, that the element `(2,4)` means (1)(2 4)(3), so as to give a cycle structure $1^2 2^1$ corresponding to $s_1^2 s_2$. The CI can also be calculated by using the GAP function `CycleIndex`, which is originally supported by the GAP system:

```
gap> G_og := Group([ (2,4), (1,2)(3,4) ]);;
gap> CycleIndex(G_og);
1/8*x_1^4+1/4*x_1^2*x_2+3/8*x_2^2+1/4*x_4
```

Then, the variable x_d is replaced by a degenerate dummy variable s_d to meet the present system of symbols.

The same CI (without CF) can be alternatively calculated by using the GAP function `CalcConjClassCICF` [23] (or `CalcCICF` [22]), which has been originally developed for calculating CI-CFs:

```
gap> Read("c:/fujita0/fujita2016/C2vsI-GAP/calc-GAP/CICFgenCC.gapfunc");
gap> G_og := Group([ (2,4), (1,2)(3,4) ]);;
gap> CalcConjClassCICF(G_og, 4, 4);
1/8*b_1^4+1/4*b_1^2*b_2+3/8*b_2^2+1/4*b_4
```

Then, the sphericity index b_d is replaced by a degenerate dummy variable s_d.

6 Relationships to be focused

6.1 Hierarchy of isomerism and isomer–classification diagrams

The hierarchy of isomerism (Eq. 1) as well as the hierarchy of equivalence classes (Eq. 2) is summarized to give the following isomer-classification scheme or diagram:

$$\left(\left\{\left\langle ([\cdots]\cdots)_{\text{I–V}}\cdots\right\rangle\cdots\right\}\cdots\right), \tag{42}$$

if the hierarchy of groups (Eq. 3) is taken into consideration. The isomer-classification diagram (Eq. 42) characterizes a nested mode of isomerism, where a pair of square brackets $[\cdots]$ represents an equivalence class of enantiomerism (i.e., a pair of enantiomers); a pair of parentheses $(\cdots)_{\text{I–V}}$ represents an equivalence class of RS-stereoisomerism (i.e., a quadruplet of RS-stereoisomers contained in a stereoisogram of type I–V); a pair of angle brackets $\langle\cdots\rangle$ represents an equivalence class of stereoisomerism (i.e., a set of stereoisomers); a pair of braces $\{\cdots\}$ represents an equivalence class of isoskeletomerism (i.e., a set of isoskeletomers); and finally, a pair of boldfaced parentheses represents an equivalence class of isomerism (i.e., a set of isomers).

If 3D proligands are considered in place of 2D proligands (as graphs) as shown in Eq. 40, Eq. 42 should be modified to give the following scheme or diagram:

$$\left(\left\{\left\langle \bullet\!\langle([\cdots]\cdots)_{\text{I–V}}\cdots\rangle\!\bullet\cdots\right\rangle\cdots\right\}\cdots\right), \tag{43}$$

where a pair of angle brackets with bullets represents an equivalence class concerning 3D proligands (e.g., *cis/trans*-isomerism).

6.2 Relationship between two promolecules as entities

The formulation of such an isomer-classification scheme or diagram as Eq. 42 or Eq. 43 enable us to specify equivalence and inequivalency with respect to a relationship between two promolecules as 3D entities.

> **Relationship between two promolecules as entities**: Suppose that one promolecule as a 3D entity as well as another promolecule to be compared is selected from the isomer-classification scheme of diagram (e.g., Eq. 42 or Eq. 43). First, a narrowest equivalence class which contains these two promolecules commonly (NEC) is selected. Then, they are concluded to be equivalent with respect to the selected narrowest equivalence class. At the same time, they are concluded to be inequivalent with respect to a subordinate equivalence class (SNEC) to the NEC. Of course, the two promolecules are equivalent with respect to the equivalence class higher than the narrowest equivalence class (NEC).

For example, let us examine Figure 4 for oxiranes with the composition A^2B^2. Compare **14** with $\overline{\mathbf{14}}$. Because the corresponding NEC is an enantiomeric relationship $[\cdots]$, they are concluded to be enantiomeric to each other. Of course, the two promolecules contained in the pair $[\mathbf{14}\,\overline{\mathbf{14}}]$ is concluded to be RS-stereoisomeric, stereoisomeric, and isoskeletomeric.

Let us next compare **14** with **16**. The corresponding NEC is a stereoisomeric relationship $\langle\cdots\rangle$, so that they are stereoisomeric to each other. Because the subordinate equivalence class (SNEC) is a pair of RS-stereoisomers, the two promolecules **14** and **16** are concluded to be inequivalent with respect to an RS-stereoisomeric relationship as well as to be inequivalent with respect to an enantiomeric relationship. The latter inequivalence with respect to an enantiomeric relationship is emphasized in the conventions of stereochemistry by referring to as being "diastereomeric" or "*cis/trans*-isomeric". However, logically speaking, the expression that **14** are **16** are diastereomeric has the same meaning that they are not enantiomeric, once judged as being stereoisomeric. This means that the terms *stereoisomeric* and *enantiomeric* are sufficient as equivalence relationships without the coinage of the term "diastereomeric" (not an equivalence relationship). It is a remarkable characteristic of the terminology of stereochemistry to lay stress on such inequivalence (difference) by the intentional coinage of a term for representing inequivalence (difference).

The comparison of **14** with **18** indicates that they are isoskeletomeric, because the corresponding NEC is an isoskeletomeric relationship $\{\cdots\}$. Because the subordinate equivalence class (SNEC) is a pair of stereoisomers, they are concluded to be inequivalent with respect to a stereoisomeric relationship as well as to be inequivalent with respect to an RS-stereoisomeric relationship or an enantiomeric relationship. In particular, they are referred to as being *constitutionally anisomeric* in order to emphasize the inequivalence under a stereoisomeric relationship.

It should be noted here that the conventional term "constitutional isomeric" concerning 2D structures (graphs) has a different connotation from the present term *constitutionally anisomeric* concerning 3D structures. After Eq. 31 (or Figure 4) is modified into

$$\Big(\big\{\big\langle([\mathbf{14}\ \overline{\mathbf{14}}])_{\mathrm{I}}\ ([\mathbf{16}])_{\mathrm{IV}}\big\rangle \quad \langle([\mathbf{18}])_{\mathrm{IV}}\rangle\big\}\Big)\ , \tag{44}$$

suppose that the equivalence class of stereoisomeric 3D structures $\big\langle([\mathbf{14}\ \overline{\mathbf{14}}])_{\mathrm{I}}\ ([\mathbf{16}])_{\mathrm{IV}}\big\rangle$ appearing in Eq. 44 degenerates into a single 2D structure $\mathbf{14}_g$ as a graph, while the equivalence class of stereoisomeric 3D structures $\langle([\mathbf{18}])_{\mathrm{IV}}\rangle$ degenerates into a single 2D structure $\mathbf{18}_g$ as a graph. These graphs are regarded as 2D entities to be examined in place of the promolecules **14** etc. as 3D entities. Thereby, the following scheme is obtained:

$$\Big(\{\mathbf{14}_g\ \ \mathbf{18}_g\}\Big)\ , \tag{45}$$

where the graphs $\mathbf{14}_g$ and $\mathbf{18}_g$ are conventionally referred to as being "constitutionally isomeric". Because these graphs $\mathbf{14}_g$ and $\mathbf{18}_g$ are isomeric (or isoskeletomeric) but different in their constitutions, the conventional term "constitutionally isomeric" should be interpreted as "isomeric with different constitutions", where their different constitutions are emphasized and their isomeric features (the same compositions) are made light of. Note that the corresponding equivalence relationship is an isomeric relationship (or an isoskeletomeric relationship), but not a stereoisomeric relationship (cf. a pair of braces and a pair of boldfaced parentheses $\Big(\{\cdots\}\Big)$ appearing in Eq. 45). The conventional expression "**14** and **18** are constitutionally isomeric" is not concerned with the relationship between 3D structures $\Big(\{\mathbf{14}\ \ \mathbf{18}\}\Big)$, but connotes Eq. 45 for 2D structures (graphs).

The conventional term "constitutionally isomeric" exhibits a characteristic of a 2D-based concept as found in Eq. 45, where "isomeric" $\Big(\{\cdots\}\Big)$ is concerned with the graphs $\mathbf{14}_g$ and $\mathbf{18}_g$, which show different constitutions (as a 2D-based concept). The 2D-based term "constitution" is implicitly transformed into the same term "constitution" as a 3D-based concept, because the 2D-based graphs $\mathbf{14}_g$ and $\mathbf{18}_g$ correspond respectively to 3D-based sets $\big\langle([\mathbf{14}\ \overline{\mathbf{14}}])_{\mathrm{I}}\ ([\mathbf{16}])_{\mathrm{IV}}\big\rangle$ and $\langle([\mathbf{18}])_{\mathrm{IV}}\rangle$. As shown in Eq. 44, the two 3D-based sets are inequivalent under a stereoisomeric relationship, where each of the two 3D-based sets is an equivalence class under a stereoisomeric relationship. They are equivalent under an isomeric relationship or an isoskeletomeric relationship.

7 Conclusion

Group hierarchy for characterizing an oxirane skeleton has been discussed by defining the point group $\boldsymbol{C}_{2v}$ for enantiomerism, the *RS*-stereoisomeric group $\boldsymbol{C}_{2v\widetilde{\sigma}\widehat{I}}$ for *RS*-stereoisomerism, the stereoisomeric group $\widetilde{\boldsymbol{C}}_{2v\widetilde{\sigma}\widehat{I}}$ for stereoisomerism, the isoskeletal group $\widetilde{\widetilde{\boldsymbol{C}}}_{2v\widetilde{\sigma}\widehat{I}}$

for isoskeletomerism. These groups are constructed as the corresponding combined-permutation representations by starting from respective sets of generators. Thereby, hierarchical enumeration of oxirane derivatives is conducted by calculating cycle indices with chirality fittingness (CI-CFs). A set of ligand-inventory functions for 3D enumerations is defined for the purpose of enumerations under the point groups $\boldsymbol{C}_2$ and $\boldsymbol{C}_{2v}$ as well as under the RS-stereoisomeric group $\boldsymbol{C}_{2v\widetilde{\sigma}\widehat{I}}$. On the other hand, a single ligand-inventory function for 2D (graph) enumeration is defined for the purpose of enumerating under the stereoisomeric group $\widetilde{\boldsymbol{C}}_{2v\widetilde{\sigma}\widehat{I}}$ and under the isoskeletal group $\widetilde{\widetilde{\boldsymbol{C}}}_{2v\widetilde{\sigma}\widehat{I}}$. The calculations of CI-CFs and of generating functions for enumeration are conducted by means of the GAP system. The enumeration results are discussed by developing isomer-classification diagrams. Thus, the data of oxirane derivatives with the composition $\mathrm{A}^2\mathrm{B}^2$, with the composition ABCD, and with the compositions $\mathrm{A}^2\mathrm{p}\overline{\mathrm{p}}$ and $\mathrm{A}^2\mathrm{p}^2$ (or $\mathrm{A}^2\overline{\mathrm{p}}^2$) are examined by drawing respective isomer-classification diagrams, where A, B, C, and D represents achiral proligands and a pair of p and $\overline{\mathrm{p}}$ represents a pair of enantiomeric proligands in isolation.

References

[1] E. L. Eliel, Infelicitous stereochemical nomenclature, *Chirality* **9** (1997) 428–430.

[2] G. Helmchen, Glossary of problematic terms in organic stereochemistry, *Enantiomer* **2** (1997) 315–318.

[3] K. Mislow, Stereochemical terminology and its discontents, *Chirality* **14** (2002) 126–134.

[4] J. Gal, Stereochemical vocabulary for structures that are chiral but not asymmetric: History, analysis, and proposal for a rational terminology, *Chirality* **23** (2011) 647–659.

[5] K. Mislow, J. Siegel, Stereoisomerism and local chirality, *J. Am. Chem. Soc.* **106** (1984) 3319–3328.

[6] V. Prelog, G. Helmchen, Basic principles of the CIP-system and proposal for a revision, *Angew. Chem. Int. Ed. Eng.* **21** (1982) 567–583.

[7] G. Helmchen, Nomenclature and vocabulary of organic stereochemistry, in: G. Helmchen, R. W. Hoffmann, J. Mulzer, E. Schaumann (Eds.), *Stereoselective Synthesis*, Georg Thieme, Stuttgart, 1996, pp. 1–74.

[8] C. Clapham, *The Concise Oxford Dictionary of Mathematics*, Oxford Univ. Press, Oxford, 1990.

[9] S. Fujita, Misleading classification of isomers and stereoisomers in organic chemistry, *Bull. Chem. Soc. Jpn.* **87** (2014) 1367–1378.

[10] S. Fujita, Classification of stereoisomers. Flowcharts without and with the intermediate concept of RS-stereoisomers for mediating between enantiomers and stereoisomers, *Tetrahedron: Asymmetry* **27** (2016) 43–62.

[11] G. P. Moss, Basic terminology of stereochemistry (IUPAC recommendations 1996), *Pure Appl. Chem.* **68** (1996) 2193–2222.

[12] D. G. Morris, *Stereochemistry*, Royal Soc. Chem., Cambridge, 2001.

[13] E. L. Eliel, S. H. Wilen, M. P. Doyle, *Basic Organic Stereochemistry*, Wiley, New York, 2001.

[14] A. von Zelewsky, *Stereochemistry of Coordination Compounds*, Wiley, Chichester, 1996.

[15] H. Hirschmann, K. R. Hanson, The differentiation of stereoheterotopic groups, *Eur. J. Biochem.* **22** (1971) 301–309.

[16] E. L. Eliel, Prostereoisomerism (prochirality), *Top. Curr. Chem.* **105** (1982) 1–76.

[17] T. W. G. Solomons, *Organic Chemistry*, Wiley, New York, 1984.

[18] K. P. C. Vollhardt, N. E. Schore, *Organic Chemistry. Structure and Function*, Freeman, New York, 2003.

[19] J. Eames, J. M. Peach, *Stereochemistry at a Glance*, Blackwell, Oxford, 2003.

[20] S. Fujita, *Mathematical Stereochemistry*, De Gruyter, Berlin, 2015.

[21] S. Fujita, Combinatorial approach to group hierarchy for stereoskeletons of ligancy 4, *J. Math. Chem.* **53** (2015) 1010–1053.

[22] S. Fujita, Computer-oriented representations of point groups and cycle indices with chirality fittingness (CI-CFs) calculated by the GAP system. Enumeration of three–dimensional structures of ligancy 4 by Fujita's proligand method, *MATCH Commun. Math. Comput. Chem.* **76** (2016) 379–400.

[23] S. Fujita, Computer–oriented representations of $\mathbf{O}_h$-skeletons for supporting combinatorial enumeration by Fujita's proligand method. GAP calculation of cycle indices with chirality fittingness (CI-CFs), *MATCH Commun. Math. Comput. Chem.* **77** (2017) 409–442.

[24] S. Fujita, Computer–oriented representations of RS–stereoisomeric groups and cycle indices with chirality fittingness (CI-CFs) calculated by the GAP system. Enumeration of RS-stereoisomers by Fujita's proligand method, *MATCH Commun. Math. Comput. Chem.* **77** (2017) 443–478.

[25] S. Fujita, Graphs to chemical structures 1. Sphericity indices of cycles for stereochemical extension of Pólya's theorem, *Theor. Chem. Acc.* **113** (2005) 73–79.

[26] S. Fujita, Graphs to chemical structures 2. Extended sphericity indices of cycles for stereochemical extension of Pólya's coronas, *Theor. Chem. Acc.* **113** (2005) 80–86.

[27] S. Fujita, Graphs to chemical structures 3. General theorems with the use of different sets of sphericity indices for combinatorial enumeration of nonrigid stereoisomers, *Theor. Chem. Acc.* **115** (2006) 37–53.

[28] S. Fujita, *Combinatorial Enumeration of Graphs, Three–Dimensional Structures, and Chemical Compounds*, Univ. Kragujevac, Kragujevac, 2013.

[29] S. Fujita, Stereoisograms for three-membered heterocycles: II. Chirality, RS–stereogenicity, and ortho–stereogenicity on the basis of the proligand-promolecule model, *J. Math. Chem.* **53** (2015) 305–352.

[30] S. Fujita, Stereogenicity revisited. Proposal of holantimers for comprehending the relationship between stereogenicity and chirality, *J. Org. Chem.* **69** (2004) 3158–3165.

[31] S. Fujita, Pseudoasymmetry, stereogenicity, and the RS–nomenclature comprehended by the concepts of holantimers and stereoisograms, *Tetrahedron* **60** (2004) 11629–11638.

[32] G. Pólya, Kombinatorische Anzahlbestimmungen für Gruppen, Graphen und chemische Verbindungen, *Acta Math.* **68** (1937) 145–254.

[33] G. Pólya, R. C. Read, *Combinatorial Enumeration of Groups, Graphs, and Chemical Compounds*, Springer, New York, 1987.

[34] S. Fujita, How many alkanes of C_nH_{2n+2} are there? — Solving a long–standing problem over 130 years, *Yuki Gosei Kagaku Kyokai-Shi/J. Synth. Org. Chem. Jpn.* **70** (2012) 951–957.